Deep-Sea Research II 134 (2016) 390–412

Contents lists available at ScienceDirect

Deep-Sea Research II

journal homepage: www.elsevier.com/locate/dsr2

Regular article

Climate to fish: Synthesizing field work, data and models in a 39-year retrospective analysis of seasonal processes on the eastern Bering Sea shelf and slope

Ivonne Ortiz [a,*], Kerim Aydin [b], Albert J. Hermann [a,j], Georgina A. Gibson [c], André E. Punt [d], Francis K. Wiese [e], Lisa B. Eisner [b], Nissa Ferm [b], Troy W. Buckley [b], Elizabeth A. Moffitt [f], James N. Ianelli [b], James Murphy [g], Michael Dalton [b], Wei Cheng [a,j], Muyin Wang [a,j], Kate Hedstrom [h], Nicholas A. Bond [a,j], Enrique N. Curchitser [i], Charlotte Boyd [d]

[a] Joint Institute for the Study of the Atmosphere and Ocean, University of Washington, Seattle, WA 98195, USA
[b] Alaska Fisheries Science Center, NOAA, 7600 Sand Point Way N.E., Building 4, Seattle, WA 98115, USA
[c] International Arctic Research Center, University of Alaska Fairbanks, Fairbanks, AK 99775, USA
[d] School of Aquatic and Fishery Sciences, University of Washington, Seattle, WA 98195-5020, USA
[e] Stantec Consulting Services Inc., 725 E Fireweed Lane, Anchorage, AK 99503, USA
[f] Sea Star Scientific Editing, Seattle, WA 98115, USA
[g] Center for Studies in Demography and Ecology, University of Washington, Seattle, WA 98195-3412, USA
[h] Institute of Marine Science, University of Alaska, Fairbanks, AK 99775, USA
[i] Department of Environmental Sciences, Rutgers University, New Brunswick, NJ 08901, USA
[j] Pacific Marine Environmental Laboratory, NOAA, 7600 Sandpoint Way NE, Building 3, Seattle, WA 98115, USA

ARTICLE INFO

Available online 16 July 2016

Keywords:
Bering Sea
Seasonal processes
End-to-end modeling
Ecosystem modeling
Pollock

ABSTRACT

We combined field data and the output from a climate-to-fish coupled biophysical model to calculate weekly climatologies and 1971–2009 time series of physical and biological drivers for 16 distinct regions of the eastern Bering Sea shelf and slope. We focus on spatial trends and physical-biological interactions as a framework to compare model output to localized or season-specific observations. Data on pollock ($\geq$8 cm) diet were used to evaluate energy flows and zooplankton dynamics predicted by the model. Model validation shows good agreement to sea-ice cover albeit with a one month delay in ice retreat. Likewise, the timing of spring phytoplankton blooms in the model were delayed approximately one month in the south and extend further into summer, but the relative timing between the spring and fall bloom peaks was consistent with observations. Ice-related primary producers may shift the timing of the spring bloom maximum biomass earlier in years when sea ice was still present after mid-March in the southern regions. Including the effects of explicit, dynamic fish predation on zooplankton in the model shifts the seasonal spring peak and distribution of zooplankton later in the year relative to simulations with implicit predation dependent only on zooplankton biomass and temperature; the former capturing the dynamic demand on zooplankton prey by fish. Pollock diets based on stomach samples collected in late fall and winter from 1982–2013 show overwintering euphausiids and small pollock as key prey items in the outer and southern Bering Sea shelf; a characteristic not currently present in the model.

The model captured two large-scale gradients, supported by field data, characterizing the overall dynamics: 1) inshore to off-shelf physical and biological differences with a gradient in inter-annual variability from higher frequency inshore to lower frequency offshore; and 2) latitudinal gradients in the timing of events. The combined effects of length of day, bathymetry, and tides, which are consistent from year to year, and the two large-scale gradients, characterize the environment on which regional differences were based and restrict their inter-annual and seasonal variability. Thus, the relative timing and sequence of events remained consistent within regions. The combination of model outputs and observational data revealed specific ecosystem processes: (1) The spatial progression in the timing, peaks and sequence of events over the shelf is driven by wind, sea ice, and stratification and creates a seasonal expansion and contraction of the warmer pelagic and bottom habitat suitable to pollock. (2) The seasonal warming of air temperature and the spring-summer expansion of the warm pelagic and bottom habitats influence the ice retreat and the associated ice edge and open water spring blooms, as well as subsequent

* Corresponding author. Fax: +1 206 526 6723.
E-mail address: ivonne@u.washington.edu (I. Ortiz).

http://dx.doi.org/10.1016/j.dsr2.2016.07.009

production/abundance of copepods and euphausiids. (3) These warmer conditions favor pelagic energy flows to pollock ($\geq$ 10 cm) and allow their distribution to expand shoreward and northward along the shelf break. (4) The fall-winter expansion of the seasonal ice cover drives the contraction of warmer waters towards the outer and southwest shelf and favors benthic energy flows over most of the shelf. There, fall blooms allow for additional lipid storage by large copepods and euphausiids that sink close to the bottom where they either go into diapause or have a restricted diel migration over winter. (5) During these cold months, the preferred pollock habitat shifts and contracts towards the outer and southwest shelf where their increased density and reduced prey availability leads to winter pollock cannibalism and consumption of overwintering euphausiids. Our project highlights the benefits of linking continuous and long-term field work with the development and implementation of highly complex models. In the face of uncertainty, simulations such as these, tightly coupled to field programs, will be instrumental as testbeds for process exploration and management evaluation, increasing their relevance for future fisheries and ecosystem management and strategic planning.

1. Introduction

The volume and value of fisheries in the eastern Bering Sea (EBS) was over a billion pounds and 1.4 billion US dollars in product value in 2014 (Fissel et al., 2015). Large and numerous populations of seabirds and marine mammals are present and utilize this area for feeding and reproduction (Friday et al., 2012; Allen and Angliss, 2012; Denlinger, 2006). The EBS has experienced shifts in the physical environment in response to the 2000-2005 warm years (Stabeno et al., 2007), including changes to circulation (Stabeno et al., 2010; Danielson et al., 2012), the extent and duration of seasonal ice coverage and subsequent variability in bottom temperatures, stratification and mixed layer depth (Hunt et al., 2011; Stabeno et al., 2012a). These physical factors affect biological productivity (Hunt et al., 2011; Stabeno et al., 2012b), fish, seabird and marine mammal distributions (Friday et al., 2013; Hollowed et al., 2012; Hunt et al., 2014; Kotwicki et al., 2005; Mueter and Litzow, 2008; Ressler et al., 2014), predator–prey interactions (Livingston and Methot, 1998; Boldt et al., 2012; Hunt et al., 2014), and survival rates and reproductive success (Heintz et al., 2013; Hunt et al., 2016).

Climate variability, and in particular climate change under the global warming background (IPCC, 2007, 2013), impacts abundance, distribution, and the commercial catch of marine resources and has thus been recognized as one of the main challenges to sustainable fisheries (Brander, 2013; Salinger, 2013). Tools that resource management agencies have employed to understand the impact of climate change on the abundance, distribution and species composition of marine resources and fisheries include, but are not limited to, spatial models, single- and multi-species stock projections with environmental forcing and/or predator/prey interactions, and spatially-explicit ecosystem models (Hollowed et al., 2011, 2013). Diverse management measures have been implemented as part of an Ecosystem Approach to Fisheries Management (EAFM) for the Alaskan groundfish fisheries for over 15 years (Witherell et al., 2000). The general framework of the ecosystem assessment has evolved from that described by Livingston et al. (2005), to the current selected suite of physical-, biological- and fisheries-related ecosystem indicators that provide the core information for an annual ecosystem report card and ecosystem assessment chapter (e.g. Zador, 2015). A multi-model approach that includes multi-species models/reference points and ecosystem models, is used to simulate future ecosystem status and policy options (Jurado-Molina et al., 2005; Ianelli et al., 2016; Moffitt et al., 2016).

End-to-end models, which incorporate processes from climate to fish at various levels of complexity, have proliferated in recent years, and have become increasingly relevant as they improved to include human dimensions, climate impacts, and processes at multiple spatial and temporal scales (Travers et al., 2007; Rose et al., 2010; Punt et al., 2016). As a result, end-to-end models that include downscaled earth systems models coupled to lower trophic level models are starting to be more commonly applied to address fisheries-management concerns – especially those models that include key fish groups (Travers et al., 2009; Kishi et al., 2011; Rose et al., 2015; Travers et al., 2014a, 2014b). End-to-end models have also been recognized as effective strategic tools and are considered essential to EAFM (Fulton, 2010; Fulton et al., 2014). Despite these advances, active research continues on refining our understanding of the linkages between climate variability and marine resources as mediated by oceanography and phytoplankton/zooplankton productivity.

As part of the Bering Sea Project, a large scale, multi-disciplinary, and multi-institutional ecosystem research program (Wiese et al., 2012), we developed (and coupled) ~10-km resolution models of the physics, lower trophic levels and key fish species in the Bering Sea. The Regional Ocean Model System (ROMS) applied to the Bering Sea (Bering10K) provides information such as currents, temperature, ice thickness and snow cover to the lower trophic level Nutrients-Phytoplankton-Zooplankton (NPZ) model developed under the Bering Ecosystem Study (BEST; ARCUS, 2004, 2005). The BESTNPZ model provides phytoplankton and ice-algae density estimates that were used to attenuate light in the Bering10K-ROMS model, thus establishing a two-way feedback between oceanography and lower trophic levels. In turn, the BESTNPZ model provides the zooplankton prey fields (euphausiids [Order Euphausiacea, krill], and small and large copepods [*Neocalanus* sp., *Calanus marshallae*, respectively]) to the Forage and Euphausiids Abundance in Space and Time (FEAST) fish model. Two-way feedback therein is enabled by applying the fish predation on zooplankton from the FEAST model to the zooplankton biomass in the BESTNPZ model. The spatially-explicit fisheries removals are included by sector, gear, and species (Fig. 1). The dual objectives for the coupled regional Bering10K-ROMS-BESTNPZ-FEAST models were to: 1) investigate biophysical processes and climate impacts; and 2) aid fisheries management by addressing both bottom-up and top-down forcing mechanisms on fish stocks and ecosystems (Wiese et al., 2012).

Here we describe the Bering10K-ROMS-BESTNPZ-FEAST model, and the physical and biological data used for comparison with, and validation of, the model output. We then present the weekly climatologies of physical and biological characteristics from a 1971-2009 hindcast of the model and highlight seasonal process in 16 distinct regions in the EBS shelf and slope. Finally, we present modeled monthly climatologies and length-based feeding habits of walleye pollock (*Gadus chalcogrammus* formerly known as *Theragra chalcogramma*, Page et al., 2013 and hereafter, pollock), based on stomach data collected from 1982 to 2013, and consider

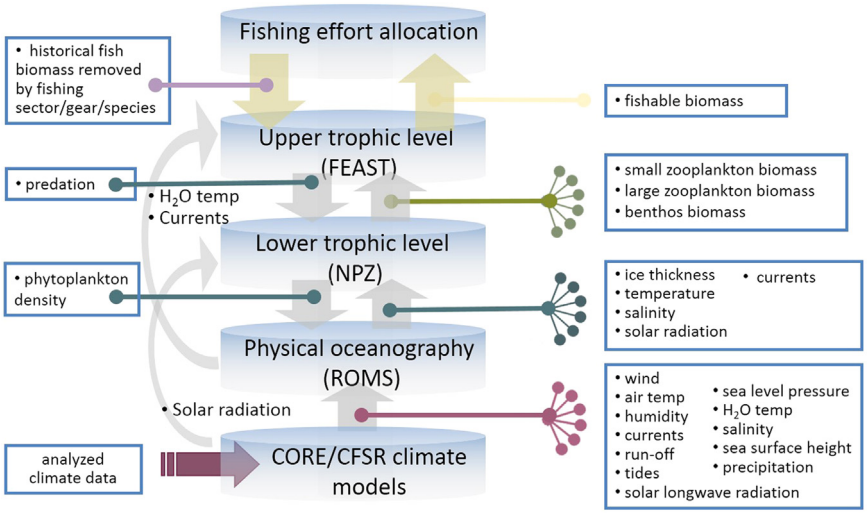

Fig. 1. Data flow and feedbacks across the components of the coupled physical-biological-fish model, Bering10K-ROMS-BESTNPZ-FEAST for the Bering Sea. The model has a spatial resolution of ~10 km and 10 vertical layers. Lower trophic levels include an ice module, nutrients, phytoplankton, zooplankton and benthos; fish include 15 species with the three main species being walleye pollock, Pacific cod and arrowtooth flounder; fishing effort is based on historical catches of 16 fisheries defined by sector, gear, and species.

how pollock respond to the seasonal processes and shifts in energy flow within the food-web.

2. Methods and model descriptions

To facilitate the comparison and synthesis of spatial patterns in both data and model output, we use the set of standard marine regions developed by Ortiz et al. (2013) as part of the Bering Sea Project and encompass the EBS shelf and slope (Fig. 2). These marine regions were chosen based on documented similarity of selected meso-scale processes and the requirement to minimize within-region variance and maximize variance across regions. The inner, middle and outer domain are shown in light, medium and dark gray, respectively. In the southeastern Bering Sea shelf, the inner and middle domains are separated by the inner front (at approximately 50 m depth), while the middle and outer domain are separated by a middle transition zone (or middle front, approximately at 100 m depth) (Coachman, 1986).

The Bering10K-ROMS-BESTNPZ-FEAST model (Fig. 1) represents the three-dimensional dynamics of the two-way interactions between physical oceanography, nutrients-phytoplankton-zooplankton, fish and fisheries. The hindcast simulation covers the years 1971 to 2009. A detailed description of the regional downscaling to the Bering Sea is given by Hermann et al. (2013, 2016). Briefly, for the years 1971-2003, we used downscaled outputs from the coupled ocean-ice Coordinated Ocean Research Experiments (CORE; Large and Yeager, 2009) as atmospheric forcing, with oceanic boundary conditions interpolated from the ROMS model for the Northeast Pacific (NEP-5, Danielson et al., 2011). NEP-5 itself utilized CORE atmospheric forcing and ocean boundary conditions derived from the Simple Ocean Data Assimilation oceanic reanalysis (SODA, Carton and Giese, 2008). We used the Climate Forecast System Reanalysis (CFSR; Saha et al., 2010) for both atmospheric forcing and oceanic boundary conditions for the years 2004-2009 as described by Hermann et al. (2013). We describe the submodules of the Bering10K-ROMS-BESTNPZ-FEAST model in the following sections.

2.1. Oceanography

The Bering10K-ROMS is a regional coupled ocean-sea-ice circulation model whose spatial domain is a subset of NEP-5, described and evaluated by Danielson et al. (2011). NEP-5 builds on a model described by Curchitser et al. (2005). The Bering10K-ROMS uses a regular grid that has a spatial resolution of ~10 km and 10 vertical layers. It extends from the western Gulf of Alaska to the Russian coast and to slightly north of the Bering Strait (Fig. 2, see inset). The Bering10K-ROMS simulation includes modifications to the heat and salinity fluxes of NEP-5, which were calibrated using extensive mooring data (Hermann et al., 2013); Hermann et al. (2016) describe additional modifications to the heat flux and ice dynamics, and conducted additional model-data comparisons for temperature and salinity; it is that version of the physical model which is utilized in the present work. Model coupling of the Bering10K-ROMS with the BESTNPZ model includes feedback from the BESTNPZ to the Bering10K-ROMS model through phytoplankton density, which affects attenuation of shortwave radiation, and thus heat absorption in the upper water column (further described in Hermann et al., 2016).

2.2. Nutrients, phytoplankton and lower trophic levels

The BESTNPZ model used is based on Gibson and Spitz (2011). It was specifically designed to incorporate the impact of ice on lower trophic levels of the Bering Sea, and includes nutrients (nitrate, ammonium, iron), ice algae, small and large phytoplankton, small copepods, oceanic and shelf large copepods, oceanic and shelf euphausiids, jellyfish (Class Scyphozoa), fast and slow sinking (pelagic) detritus, benthic detritus and benthic infauna (Fig. 3). Zooplankton are distributed throughout the water column (only the large copepods vertically migrate), and biomass is tracked for micro and mesozooplankton. In the BESTNPZ model, the lifespan of euphausiids is implicitly a year (but has been recorded to be longer in higher latitudes, [Dalpadado and Skojdal, 1996; Hunt et al., 2016]) because their biomass (as for all the zooplankton groups) approaches zero every winter. Both mortality and respiration exceed growth, reflecting the understanding of euphausiid biology in the region when the model was initially constructed rather than the more recently understood overwintering dynamics (Orlova et al., 2014; Huenerlage et al., 2015).

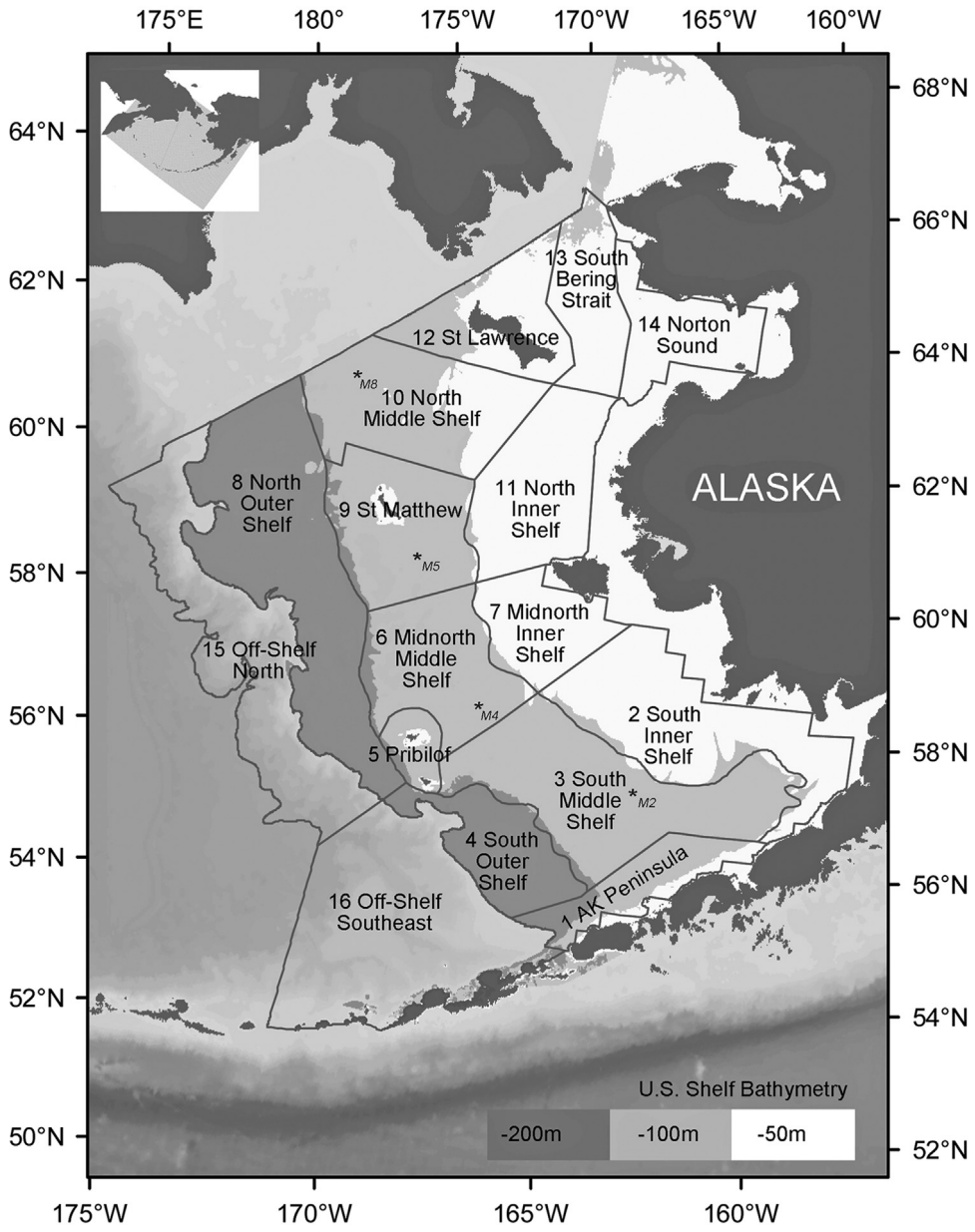

Fig. 2. Marine regions used for spatial averaging of results (from Ortiz et al., 2013). Asterisks show Moorings M2, M4, M5 and M8, which are located along the 70 m isobath. Inset map shows extent of the Bering10K-ROMS-BESTNPZ-FEAST model.

Spatio-temporal dynamics of the BESTNPZ model are affected by ice thickness, temperature, salinity, solar radiation, and circulation patterns provided by the Bering10K ROMS model (Fig. 1). The compartments used as food supply for fish in the FEAST model are the euphausiids, copepods and benthic infauna (Fig. 3).

The total mortality of zooplankton groups and benthic infauna is modeled as a tuned quadratic function of temperature and zooplankton biomass when the BESTNPZ model (Gibson and Spitz, 2011) is not coupled to the FEAST model. When the Bering10K-ROMS, BESTNPZ and FEAST models are fully coupled, zooplankton mortality is a combination of fish predation calculated using the fish length-based bioenergetics model (Section 2.3), and an additional 'other natural mortality' that is a reduced value of the quadratic mortality utilized in the uncoupled version. It is assumed that fish can prey on zooplankton throughout the water column so fish consume zooplankton from all layers proportional to their layer-specific density even though the FEAST model has no vertical fish distribution.

2.3. Fish

The FEAST model is a 2-dimensional (2D), gridded, daily-scale multispecies length-based foraging, bioenergetics movement, and recruitment model for post-larval forage and predatory fish. It runs within the Bering10K-ROMS framework, with fish as state variables being tracked as 2D biological tracers. Fish numbers, condition factor and caloric density are driven by inputs of prey availability, depth-averaged temperature, and water movement (i.e. advection) from the Bering10K-ROMS-BESTNPZ model. The depth-averaged temperature is used in temperature-dependent functions for prey-consumption and metabolism (Fig. 1). FEAST obtains daily estimated dry weight of euphausiids, small copepods, large copepods, and benthic infauna from the BESTNPZ

model and produces daily mortality rates for prey, which can be fed back into the BESTNPZ model as biomass consumed by fish for each zooplankton species and benthic infauna. This results in a two-way coupled modeling structure between plankton and fish. The conversion from BESTNPZ dry weight to FEAST wet weight and caloric density is calculated according to pre-specified species-specific ratios. This is because there is no way of allocating consumption to growth, reproduction and increased caloric density for biomass pools without introducing *a priori* assumptions regarding the effects of environmental factors. Table 1 lists the species included in the version of FEAST described here. FEAST also models spatially-distributed fleet-specific fisheries, driven by historical spatial reconstructions of Bering Sea fisheries on a weekly resolution.

2.3.1. Fish population dynamics and foraging

Each fish species in FEAST is divided into length bins. For some species, a separate set of length bins are used for each fish-age class, covering ages 0 through 10+; for others, there is no tracked age structure (Table 1, Fig. 4). For fish age-1 and older, 4 cm width fork length bins are used; for age-0 fish or fish without age structure, 2 cm width fork length bins are used. All fish in a length bin are assumed to have the midpoint length for that bin. All fish in the model, including the smallest age-0 length bin (0–2 cm), are considered "post-larval" (discussed below).

Three state variables are tracked at each horizontal ROMS grid location for each fish-length bin: 1) numbers of fish per m^2; 2) individual fish wet weight (tracked as condition factor, a ratio representing deviation from an established fixed length/weight relationship); and 3) fish caloric density (joules per gram of fish wet weight).

For each daily time step and each length bin of fish, the model first calculates the available prey for that length bin of fish as the sum of the prey's biomass (across all prey, including zooplankton and other fish bins) multiplied by a length- and species-based selectivity function (gamma selectivity based on the log of the ratio between predator and prey lengths; Kinzey and Punt, 2009). For zooplankton, we used fixed mean prey lengths based on pollock stomach samples collected in 2009-2010 (Buckley et al., in preparation).

The daily consumption, respiration, and therefore net growth (in joules) for each fish length box is calculated using a visual foraging model (e.g. Ware, 1978), which is based on the available prey, combined with a temperature-dependent bioenergetics model of respiration (Ciannelli et al., 1998). This output is used to

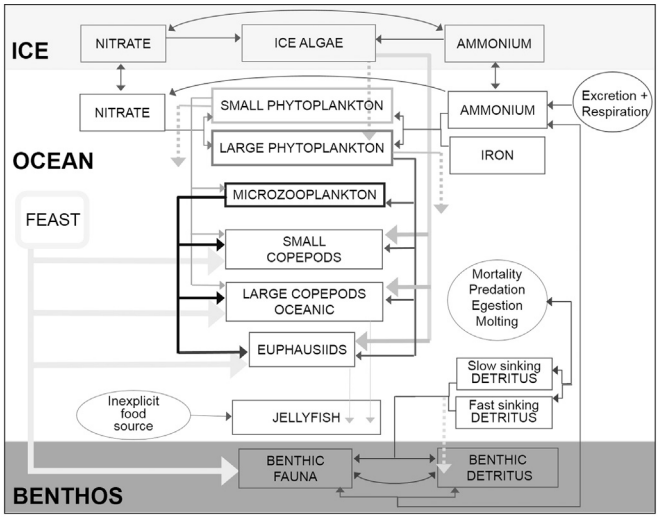

Fig. 3. Nutrient-Phytoplankton-Zooplankton model for the Bering Sea (BESTNPZ, based on Gibson and Spitz, 2011).

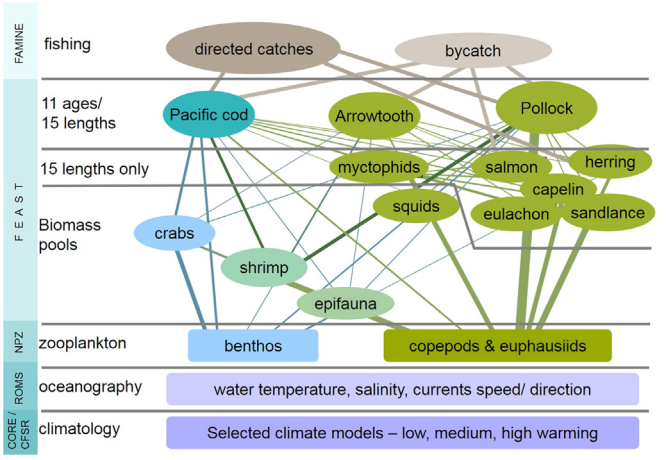

Fig. 4. Trophic structure and coupled processes represented in the Bering10K-ROMS-BESTNPZ-FEAST model. Note not all fish groups have the same level of modeling detail.

Table 1
List of groups in and their population structure assumed in the FEAST model. M = mortality, G = growth, R = recruitment, Mov = movement.

Group name	Species	No. age classes	No. length classes	Length interval (cm)	Processes explicitly modeled
Pollock age-1 and older	*Gadus chalcogrammus*	10	14	4	M, G, R, Mov
Pollock age-0		1	20	2	M, G, R, Mov
Pacific cod age-1 and older	*Gadus macrocephalus*	10	14	4	M, G, R, Mov
Pacific cod age-0		1	20	2	M, G, R, Mov
Arrowtooth flounder age-1 and older	*Atherestes stomias*	10	14	4	M, G, R, Mov
Arrowtooth flounder age-0		1	20	2	M, G, R, Mov
Pacific herring	*Clupea palassi*	–	20	2	Mov
Capelin	*Mallotus villosus*	–	20	2	Mov
Eulachon	*Thaleictes pacificus*	–	20	2	Mov
Pacific Sandlance	*Ammodytes hexapterus*	–	20	2	Mov
Myctophid	*Myctophidae*	–	20	2	–
Squid	*Order Teuthida*	–	fixed at 10		–
Crabs	*Chionecetes opilio*	–	fixed at 2		–
Shrimp	*Pandalidae*	–	fixed at 2		–
Epifauna		–	fixed at 1		–
Misc. zoop.		–	fixed at 2		–

calculate the ideal "foraging activity level" for the predator by assuming this activity level is linked to swimming velocity (affecting the amount of energy captured) and respiration (affecting the cost of capture). The combination of prey length-based selectivity and foraging energy maximization allows the model to capture "emergent" prey-switching behavior.

Once daily rates (e.g. consumption, respiration) are calculated, net fish growth is computed within the model either by transitioning a proportion of numbers of fish per unit area from a bin to a larger length bin (representing growth in length), or by increasing condition factor (and therefore weight-at-length) or caloric density (and therefore caloric density-at-length) according to an allocation schedule adjusted to match historical data. Net energy losses are dealt with either by decreasing condition factor or caloric density (fish cannot decrease in length). If the condition factor or caloric density for a particular fish-length bin drops below a minimum, the fish starve and are removed from the model (numbers of fish per m^2 set to zero). Mortality rates are then applied to the prey in the model given the amount of consumption calculated. While the rates are calculated daily, the state variables may be integrated on a finer timestep to match concurrent physics or BESTNPZ simulation. However, this does not imply that FEAST is designed to produce sub-daily results (e.g., diel feeding is not included).

Finally, the spawning biomass for an age-structured species in a grid cell is calculated by applying length-based maturity and fecundity curves to each length bin. "Spawning" fish convert caloric energy to "eggs" according to a fixed seasonal reproductive schedule from laboratory data (Buckley and Livingston, 1994). A fixed mortality rate is applied to the total number of eggs estimated from spawning fish. The surviving "eggs" for a species are modeled as a single quantity for each 2D cell and do not interact with other species or experience mortality, but are advected by water-column averaged velocities based on the underlying physical model. Within each cell, a proportion of the number of eggs is converted to numbers of fish age-0 across a fixed range of dates annually, at which point the fish are normally distributed across the smaller 2 cm size bins (out of 20).

2.3.2. Fish movement

Fish movement between neighboring horizontal grid cells is based on fish length, the spatial gradient of habitat quality and a diffusion rate inversely proportional to the local habitat quality (i.e., the steeper the habitat gradient, the faster fish swim towards the higher quality habitat). Due to the numerical integration timestep and the coarseness of the grid (10 km), there might be isolated instances when a small fraction of fish moves across grid cells faster than their swim speed. Habitat quality for each fish-length bin is defined as a function of net change in fish population energy, itself a product of individual net energy gain and predation mortality expressed in the same units. It is important to note that this "swimming rate" is not linked to the foraging effort (swimming velocity) mentioned above.

2.3.3. Fishing effort allocation

Fish can disappear from the model due to natural mortality or starvation, as explained above, but also due to fisheries. The fishing effort allocation for the hindcast is based on historical sector/gear/species catch data downscaled to weekly removals by Alaska Department of Fish and Game STAT6 statistical areas. Standard ADFG STAT6 areas are 0.5° latitude by 1.0° longitude when no land masses intersect (ADFG, 2011). The nominal STAT6 areas around land masses (e.g., the Alaska Peninsula) are irregularly shaped to conform to the land mass boundary and often much smaller than standard STAT6 areas. A uniform grid of standard size STAT6 covering the extent of the Bering grid was created to simplify the spatial distribution of catches. Land-free STAT6 areas were not affected by this, but irregular STAT6 areas were assigned to the overlapping STAT6 areas from the uniform grid (Boyd et al., 2014). Removals in each uniform STAT6 area were further downscaled to the FEAST grid (in this case the horizontal Bering10K grid), by allocating removals proportional to the biomass at the start of each week in each FEAST grid cell.

Catch input from historical data is in biomass by species. This is converted to removal rates (reduction rates in numbers) for particular fish length bins using fixed gear/species length selectivity curves generated from stock assessments. The fisheries are specified by sector (catcher-processors and catcher-vessels), target species and gear. The fisheries included are: catcher-processor for pollock trawl, Pacific cod trawl, pots and longline, other species trawl, pots and longline, herring gillnets and seine.

2.4. Initial conditions and field data

Although the fish can move throughout the total grid, the area of interest is restricted to the EBS shelf/slope regions, with a depth cutoff of 200 m for the shelf and 3,500 m for the slope. The northern shelf boundary corresponds to the U.S. Exclusive Economic Zone, and the farthest southwest (Aleutian) point corresponds to 172 °W along the Aleutian Archipelago (Fig. 2). This area is seeded with fish for the initial conditions. The FEAST model needs starting conditions for each of three state variables: 1) numbers of fish per m^2; 2) individual fish wet weight; and 3) fish caloric density for each fish species. For all fish, the initial condition factors were assumed to be 1 and initial energy density was assumed to be the mean caloric density-at-length. Initial conditions for the fish were derived from the historical database of the RACE (Resource Assessment and Conservation Engineering Division) Bottom Trawl summer Survey (BTS) conducted by the Alaska Fisheries Science Center (AFSC) and stock assessment estimates in the case of pollock, cod, arrowtooth, and herring. When needed, stock assessment estimates were scaled in proportion to the biomass in the BTS that fell outside the assumed distribution of the fish stock in the stock assessment used (e.g., arrowtooth estimates were scaled down to account for fish in the Aleutian Islands). The numbers of fish-at-age were converted to numbers of fish-at-age and -length based on long term length distributions for each age estimated from a historical database maintained by the AFSC Resource Ecology and Fisheries Management division's Age and Growth Program (http://www.afsc.noaa.gov/REFM/Age/). For the initial conditions, we allocated the number of fish-at-length estimated for 1971 from the stock assessment using the mean spatial distribution by length derived from the BTS based on "average" years (1996, 2000, and 2006). The warm/cold/average year classification follows Stabeno et al. (2012a, 2012b), who defined "average" years as those when daily and monthly water column temperatures were close to their corresponding 1995-2010 mean at mooring M2. If no fish of a given size were recorded at the station in the BTS corresponding to a location in the model, then the number of initial fish for that bin at that location was set to zero. No adjustment was made for length selectivity of the BTS. Total biomass for species with no age structure was allocated using the mean spatial biomass distribution in the BTS of average years scaled by a catchability factor estimated from survey biomass estimates and the group's biomass as estimated by an ecosystem mass balance model for the EBS (Aydin et al., 2007). Total numbers of fish per m^2 for species with no stock assessment were estimated based on survey data: total BTS biomass as scaled by the catchability, converted to numbers of fish-at-length. For this conversion we assumed a length-based population structure at equilibrium and multiplied it by the

Table 2
Data used for fish initial conditions. RACE= Resource Assessment and Conservation Engineering Division of the Alaska Fisheries Science Center (AFSC); AGP= Age and Growth Program of the AFSC; BTS=Bottom Trawl Survey; BASIS=Bering-Aleutian Salmon International Survey; q is the catchability coefficient as estimated for given species/group from BTS estimates and biomass as estimated by the mass balanced model for the eastern Bering Sea, Aydin et al, 2007).

Group	Numbers/Biomass	Spatial distribution	Length
Pollock	Stock assessment estimate for 1971 (NPFMC, 2009) plus 2% assumed to inhabit the Northern Bering Sea (based on survey ratio between north and south strata)	RACE mean average year	Length-at-age data from RACE AGP, BTS and BASIS
Cod	Stock assessment estimate for 1971 (NPFMC, 2009)	RACE mean average year	Length-at-age data from RACE AGP, BTS and BASIS
Arrowtooth flounder	Back calculation of numbers-at-age from the stock assessment estimate for 1982 (NPFMC, 2009) less 17% outside the Bering Sea shelf and slope.	RACE mean average year	Length-at-age data from RACE AGP, BTS and BASIS
Herring	Back calculation of numbers-at-age from the stock assessment estimate for 1982 stock assessment (Salomone et al., 2011)	RACE mean average year	Length at age data from RACE survey
Capelin	Survey estimate in biomass for 1982 *q from Ecopath converted to numbers of fish using a length-weight relationship and assuming population at equilibrium	RACE mean average year	Length data from RACE survey
Eulachon	Survey estimate in numbers for 1982*q from Ecopath	RACE mean average year	Length data from RACE survey
Sandlance	Survey estimate in numbers for 1982*q from Ecopath	RACE mean average year	Length data from RACE survey
Myctophids	Ecopath biomass estimate converted to numbers of fish using a length-weight relationship and assuming the population is at equilibrium	RACE mean average on shelf; uniform distribution off-shelf	Weight at length data from RACE BTS and slope survey
Squid	Ecopath biomass estimate from Aydin et al. (2007)	RACE mean average on shelf + uniform distribution off- shelf	RACE BTS and slope survey
Shrimp	Survey estimate in biomass for 1982*q from Ecopath	RACE mean average year	Length data from RACE BTS
Crab	Survey estimate in biomass for 1982*q from Ecopath	RACE mean average year	Length data from RACE BTS
Epifauna	Survey estimate in biomass for 1982*q from Ecopath	RACE mean average year	Length data from RACE BTS

corresponding longterm length-weight relationships. Table 2 summarizes the source information for the initial conditions.

2.5. Model simulation

The Bering10K-ROMS-BESTNPZ models were initialized using time-specific conditions from the hindcast by Hermann et al. (2016), which uses the same model parameterizations. We started the model on July 1, 1970, and ran a simulation with fish movement, but no mortality or growth, through December 31, 1970 (fish spin-up). Starting January 1, 1971 the fish mortality and growth were turned on for the remainder of the simulation (Jan 1, 1971–December 30, 2009). A forcing file containing daily catches by sector, gear, species, and length for each grid cell supplied the catch data for the calculation of the fishing effort. A second forcing file supplied the estimated age-1 recruits from the (EBS area-integrated) stock assessment for pollock, Pacific cod and arrowtooth flounder. At the start of each year, the total number of age-0 fish (estimated based on fecundity of mature fish and distributed according to the location of spawning fish), were corrected to that of the stock assessment estimate, while preserving the spatial distribution of the model output. Due to a lack of sufficient data on life history rates and movement, the population structure of species with no stock assessment was assumed to be static; species with no length structure were considered sessile.

2.6. Data and model validation

First we evaluated the model performance for physics, phytoplankton, and pollock. We focused model-data comparisons on key physical and biological parameters, namely sea-ice cover, chlorophyll-*a* concentrations, and timing of spring and fall blooms at moorings 2, 4, 5, and 8 (M2, M4, M5 and M8, see Fig. 2 for locations). The moorings have been described in detail in Stabeno et al. (2012a, 2012b) and are maintained by NOAA/Pacific Marine Environmental Laboratory, with the first mooring (M2) deployed in 1995. We also compared the annual number of age-1 and older pollock from the FEAST outputs to those estimated by the stock assessment for the EBS pollock (Ianelli et al., 2011). Second, since our model includes fish, we addressed whether adding fish predation makes a difference in the zooplankton biomass as estimated using only quadratic mortality.

2.6.1. Sea-ice

We used data presented in Sigler et al. (2014) to compare with weekly sea-ice cover model output to examine sea-ice variation along the 70-m isobath. This dataset is based on data from the National Ice Center (NIC), which covers the period 1971-2005 and from the Advanced Microwave Scanning Radio-EOS for the period 2002-2012. The values from both data series are very similar for the overlap years 2002-2005 (Stabeno et al., 2012b), and the average of both datasets was used. A box of 100 kmx100 km was defined around each of the four moorings, and daily values were computed from 1996-2009 and weekly averages derived. Ice was present all years at moorings M8 and M5, but was absent at M4 during 2001 and 2005, and at M2 during 1996, 2001, and 2003 – 2005 (Sigler et al., 2014).

2.6.2. Chlorophyll-a concentrations

We used daily averages of shallow (~10 m) chlorophyll-*a* concentration (Chl*a*, mgC/m^3) for the period 1996–2009 from Sigler et al. (2014) to estimate weekly averages. The data are fully detailed in Sigler et al. (2014). Briefly, the time series focuses on mooring data at 11 m (or the shallowest instrument at M5 and M8) and additional chlorophyll-*a* fluorescence measurements and water samples taken during hydrographic casts conducted when the moorings were deployed and recovered. Both moored and hydrographic chlorophyll-*a* fluorescence (volts) were converted to chlorophyll-*a* concentration ($\mu g\, l^{-1}$) using factory calibration (which has significant error). Chlorophyll-*a* estimates based on fluorescence sensors were compared to those from the water samples taken during the hydrographic casts for quality control of the mooring-based measurements; unusual values or irregular spikes were excluded as were data where measurement drift occurred.

2.6.3. Timing of spring and fall bloom

We compared the time-series of the weekly total phytoplankton biomass (ice algae, large and small phytoplankton, g C/m^2) of the top 10 m as estimated by the model to the corresponding time series of chlorophyll-*a* estimates presented by

Sigler et al. (2014) to evaluate model performance in the timing of the spring and fall bloom, as well as their relative magnitude. Time series were based on values at the mooring locations (M2, M4 between 1996–2009, M5 and M8 between 2004 and 2009). We use the temporal thresholds for determining spring and fall blooms proposed by Cheng et al. (2016) to identify the time of spring and fall bloom maxima: spring blooms are those occurring on or before Julian day 200 (or week 29); fall blooms are those occurring on or after Julian day 230 (week 33). These thresholds are 20 days later than those used by Sigler et al. (2014) based on the observational data to account for the delay in ice retreat in the model (Julian day 180 for spring bloom and 210 for fall). The 30-day interval between is the same (Cheng et al., 2016).

2.6.4. Pollock abundance

We evaluate FEAST model performance for the abundance of age-1 and older pollock by comparing the total modeled number of fish age-1 and older by year from 1971-2009 to the number of fish as estimated for the same period by the pollock stock assessment for the EBS (Ianelli et al., 2011). The time-series of modeled numbers-at-age were calculated by extracting the model output corresponding to regions 1 through 16 (Fig. 2), the assumed distributional area for the EBS pollock. We focus on pollock abundance as a key validation because they comprise the largest fish biomass in the EBS, and are the primary consumers of zooplankton (Aydin et al., 2007).

2.6.5. Difference between one-way and two-way feedback for NPZ-FEAST coupling

To determine the impact dynamic fish predation can have on modeled zooplankton biomass, we computed and then compared weekly climatologies of aggregated zooplankton (large copepods and euphausiids) within the primary habitat for pollock (>20 cm), for both one- and two-way feedback simulations (see Section 2.2). Primary habitat is defined as the area between 2 °C and 6 °C (Barbeaux, 2012) in regions 1 through 9.

2.7. Analysis – weekly climatologies of physical and biological model output

Weekly climatologies of physical and biological variables for the 16 standard marine regions (Fig. 2) were calculated for the 1971–2009 fully coupled (including fish predation) modeled time series. Averages by Julian week were used, resulting in a final week of each year being 8 days (9 in a leap year). The physical variables evaluated included: fraction of sea-ice cover and depth-integrated temperature. The biological variables included biomass of: ice algae, large and small phytoplankton, microzooplankton, small copepods, large oceanic/shelf copepods, and euphausiids. All variables constitute integrated values per m^2 over the upper 300 m (or the total depth of the water column, whichever was shallower). Weekly anomalies for the 1971–2009 time-series for the 16 regions were also calculated for the euphausiid biomass in the upper 300 m as well as for the depth-averaged temperature in the upper 300 m.

2.7.1. Monthly and seasonal climatologies of copepods, euphausiids and pollock in stomach samples of pollock length 8–80 cm

There are no direct zooplankton observations in the Bering Sea in winter and so the model assumes that biomass approaches zero and are thus not available for consumption by fish. To evaluate the concordance between model assumptions and observed availability of large zooplankton to pollock, we used information from pollock stomach samples collected throughout the year on the eastern Bering Sea shelf and slope by a variety of surveys from 1982 to 2013. This also serves the purpose of establishing a baseline year-round availability of zooplankton. The fish food habits database is maintained by the Resource Ecology and Ecosystem Modeling group of the NOAA/AFSC (http://www.afsc.noaa.gov/REFM/REEM/Data/default.htm). The data were allocated to the corresponding marine region in Fig. 2 based on the haul location where the samples were collected. First, we computed the monthly averages of frequency of occurrence of pollock, copepods (any size), and euphausiids in pollock diets for each region with at least 100 samples in any given month. Then, we calculated the seasonal contribution of each of these three prey categories to pollock diet as a function of predator (pollock) length in each region where there were at least 300 samples for each seasonal diet. Seasons were defined as the corresponding quarter in a year: Jan–Mar (winter), Apr–Jun (spring), Jul–Sep (summer), and Oct–Dec (fall).

3. Results and discussion

We present and discuss results in three sections: the first section addresses model performance; the second addresses the data from the pollock stomach samples; and the third section addresses the weekly climatologies for modeled physical attributes, phytoplankton and zooplankton, across regions.

3.1. Model performance

3.1.1. Sea-ice cover

Danielson et al. (2011) showed NEP-5 closely reproduces ice cover (expressed as percent ice concentration) and spring ice retreat onset. Model outputs for depth-integrated temperature at two southern moorings (M2 and M4) run slightly warmer in winter (up to 2 °C, Fig. 4 of Hermann et al., 2016), though near-surface temperatures can be colder than observed in the northern Bering Sea (Hermann et al., 2016). Weekly climatologies of area averaged sea-ice concentration from satellite data and the Bering10K-ROMS-NPZ-FEAST model simulations are shown in Fig. 5 for the 100 km x 100 km boxes around each mooring site. Measured and modeled ice cover are maximal between weeks 6 through 19 (Feb-May), with maximum ice cover increasing from south to north (M2 to M8). When sea ice is present, averaged sea-ice cover typically remains below 50% in the south (M2, M4) and is usually above 50% in the north (M8) and in the transition area (M5). Although the onset of sea ice retreat in the model matches observations, the model is generally not ice free until mid-June to early July at all moorings. Whereas observations, on average, show sea-ice cover is gone between week 17 (late April) at M2 and week 24 (mid-June) at M8. The difference between observed and modeled sea-ice cover at M8 ranges between 38% and 1%. The model also calculates the onset of ice cover one (M2, M4, M5) or two (M8) weeks earlier than observed.

The late ice melt delays the timing of the spring bloom (Fig. 6). Cheng et al. (2016) evaluated spring and fall blooms in the eastern Bering Sea using output from the ROMS-NEMURO-NEP model, and suggested the lack of ice algae in the NEMURO model (Kishi et al., 2007) as one potential contributing mechanisms to the slower sea-ice retreat. Our BESTNPZ model has an ice module that explicitly includes ice algae as well as feedback between the phytoplankton density and shortwave absorption. This suggests the slow sea-ice retreat is probably caused by other internal model features as suggested by Danielson et al. (2011), (e.g. the ice code utilized by Bering10K and NEP-5 had sea ice melting only at the ice-ocean interface but not at the ice-atmosphere interface), or may be inherited from global climate models used for atmospheric forcing and boundary conditions, as suggested by Cheng et al. (2016).

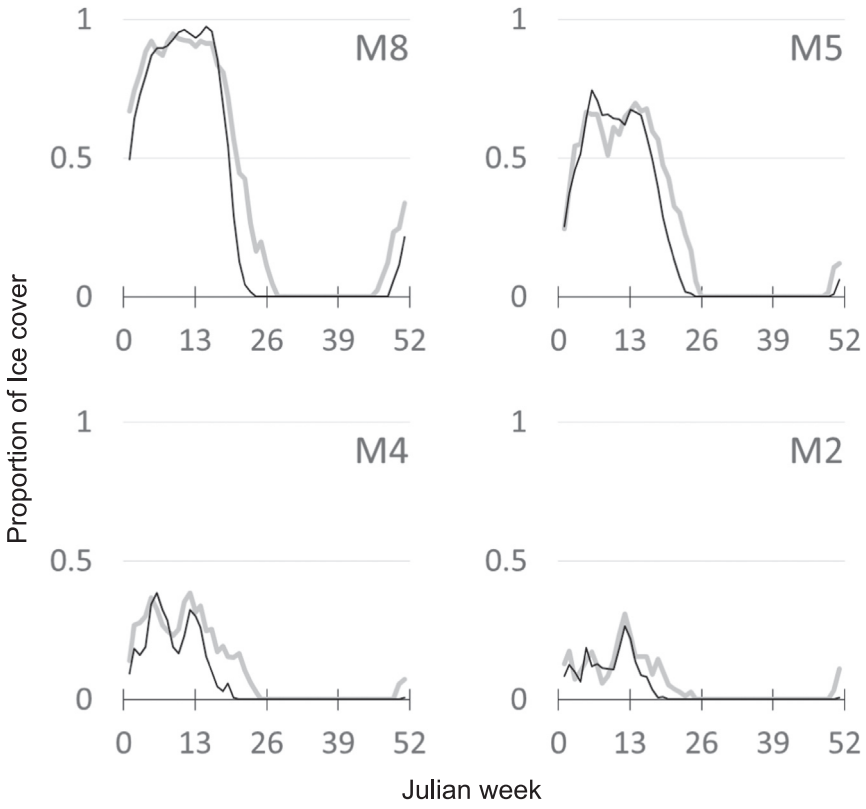

Fig. 5. Weekly climatology of ice cover averaged over a 100 km x 100 km box around the four mooring sites (M2, M4, M5 and M8). The Bering10K-ROMS-NPZ-FEAST model simulation (gray line) and satellite observations (thin black) were computed over years 1996–2009.

3.1.2. Spring and fall bloom relative magnitude and timing

Annual time series of weekly mean observed chlorophyll-*a* (Chl*a*, mgC/m^3) and total modeled phytoplankton (large+small) biomass (gC/m^2) at four moorings are shown in Fig. 6 (top two rows). In general, the model shows interannual variability of phytoplankton biomass evident in the observations, albeit the magnitudes and timing differ from observations. The relative onset and peak of the modeled spring bloom compared to observed data is generally on time for the north moorings M5 and M8, where spring blooms are ice-related; we note the blooms tend to last longer in the model compared to the observed data. In contrast, the peak biomass of spring blooms at M2 and M4 can be either ice-related (earlier in the year) or open water (later in the year when ice retreated early) (Sigler et al., 2014). These two types of blooms show up in the climatology at M2 and M4 based on chlorophyll data (bottom row Fig. 6), but is clearly not captured in the model, as shown by the weekly climatology of total phytoplankton biomass. In the model, the timing of ice algae does indeed happen earlier in the year compared to the timing of either small or large phytoplankton, however its biomass is so small it gets overwhelmed and thus has little effect on the timing of the spring bloom. The climatology of the fall bloom based on data, shows a north to south gradient in both its timing and magnitude. It is almost nonexistent at M8 (north) but it progressively increases and occurs later at M2 where the fall bloom can reach spring-like magnitudes. In contrast, the modeled fall bloom always has a magnitude matching or exceeding that of the modeled spring bloom. These discrepancies in the timing of the blooms seem partly due to the difference between the observed and modeled timing of ice retreat, where modeled sea-ice retreat is delayed in the spring, and the onset of sea ice is earlier in the fall. The interval between the timing of the maximum spring bloom and the maximum fall bloom is similar between the observed data and the modeled climatologies, however the modeled blooms appear to have a longer duration.

In general, the spring-to-fall ratio of maximum phytoplankton biomass in the model is either lower or inverse compared to the spring-to-fall ratio of the observed chlorophyll-*a* (rows 3 and 4 in Fig. 6). Both time series potentially have biases. For the model time series, lower spring maxima than those in fall could result from low values of ice algae biomass in early spring, high biomass values of small phytoplankton in fall (Fig. 6, bottom 2 rows), or a combination of both. In the observed data, the mean maximum spring chlorophyll-*a* concentration is always higher than the fall maximum, and the spring to fall ratio increases towards the north as fall blooms in the north tend to have a lower magnitude than in the south. The latitudinal gradient in the observed data might be overestimated due to: the lack of data during 1996-2003 at M5 and M8, and/or the likely biased Chl*a* measurements based on factory calibrations using spectral fluorescence signals defined on different phytoplankton communities or different physiological states of the phytoplankton (Escoffier et al., 2015) than those in the EBS at time of sampling. In general, neither the observed magnitude of the spring-to-fall peak biomass ratio, nor its latitudinal gradient, is adequately captured by the model.

The phytoplankton biomass in the model could further be biased due to: high assumed doubling rates; the emergent low grazing rates by micro-zooplankton; overestimation in nutrient availability; and/or an oversimplification of fixed carbon to chlorophyll-*a* for each phytoplankton size group, which does not permit an evolution in the ratio of carbon to chlorophyll-*a* within a species group as environmental conditions change. The influence by light, cell size, and other factors on the quantitative relationships between the C and Chl*a* needs to be incorporated into the model. Lomas et al. (2012) estimated an average C:Chl*a* ratio of 50, in spring and summer of 2008 and 2009, regardless of sampling depth, cell size or nutrient status; when the samples were parsed

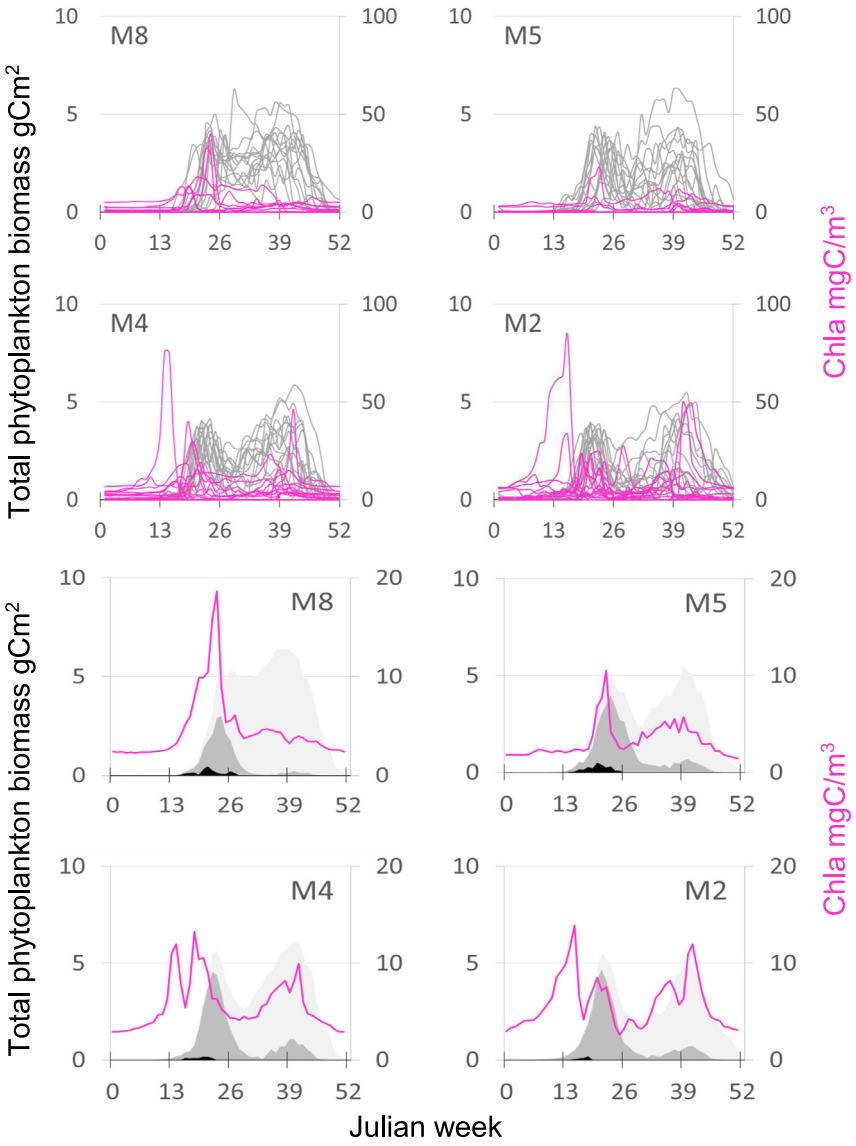

Fig. 6. Top 2 rows: annual time series of weekly mean observed chlorophyll-*a* (Chl*a*, mgC/m^3) at 10 m (pink) versus model phytoplankton (gray; large+small) biomass (gC/m^2) at moorings M2, M4, M5, M8. Bottom 2 rows: weekly climatologies of observed chlorophyll-*a* at 10 m (Chl*a*, mgC/m^3) (pink, note change in scale) versus model primary producers biomass (gC/m^2) (black – ice algae; dark gray – large phytoplankton; light gray – small phytoplankton) at moorings M2, M4, M5, M8. Time series and weekly climatologies were computed from 1996 to 2009; no observations were available for moorings M5 and M8 prior to 2004. (For interpretation of the references to color in this figure legend,the reader is referred to the web version of this article.)

by depth, size or nutrient status, the average values did vary according to expectations (e.g. small cells, <5 μm, had a higher C:Chla ratio than large cells, >5 μm), but the differences were not significant. Even if assumed significant, the difference in the C:Chl*a* ratios of large and small cells are insufficient to specify the difference in magnitude between the maximum spring (mostly large cells) and fall blooms (mostly small cells). Moreover, using higher fixed C:Chl*a* ratios for small phytoplankton and lower C:Chl*a* ratios for larger phytoplankton would still not address the latitudinal gradient in the maximum spring to fall bloom observed in the data.

Regardless of the mechanism leading to the low ice algae and high small phytoplankton biomass in the model, the ratio among the primary producers is biased and their total biomass, as calculated in the model, is likely lower in early spring and higher in fall than it should be. Both the difference in the timing of the blooms, as well as the overestimated ratio of the spring versus fall phytoplankton biomass, are evident regardless of whether comparisons are based on Chl*a*, satellite images http://www.science.oregonstate.edu/ocean.productivity/standard.product.php or net primary production derived from ocean color estimates (Brown et al., 2011).

3.1.3. *Spring bloom timing and sea ice retreat*

The model did not replicate the late ice-retreat early-spring bloom maxima behavior, despite capturing the seasonal variability of the timing of ice retreat. We explore this discrepancy further in Fig. 7 using scatterplots of the timing of maximum spring bloom (defined as the Julian week when Chl*a* or phytoplankton biomass was at its maximum during spring) versus timing of sea-ice retreat (defined as the week when sea-ice cover fell below 15%). The top row in Fig. 7 shows the scatter plots using the observed data from Sigler et al. (2014). Chlorophyll-*a* measurements do not provide any information on the autotrophs contributing to the chlorophyll pool, so rows 2 to 5 (Fig. 7) show the timing of the maximum phytoplankton biomass in spring of ice algae only (row 2), large phytoplankton only (row 3), the sum of ice algae and large

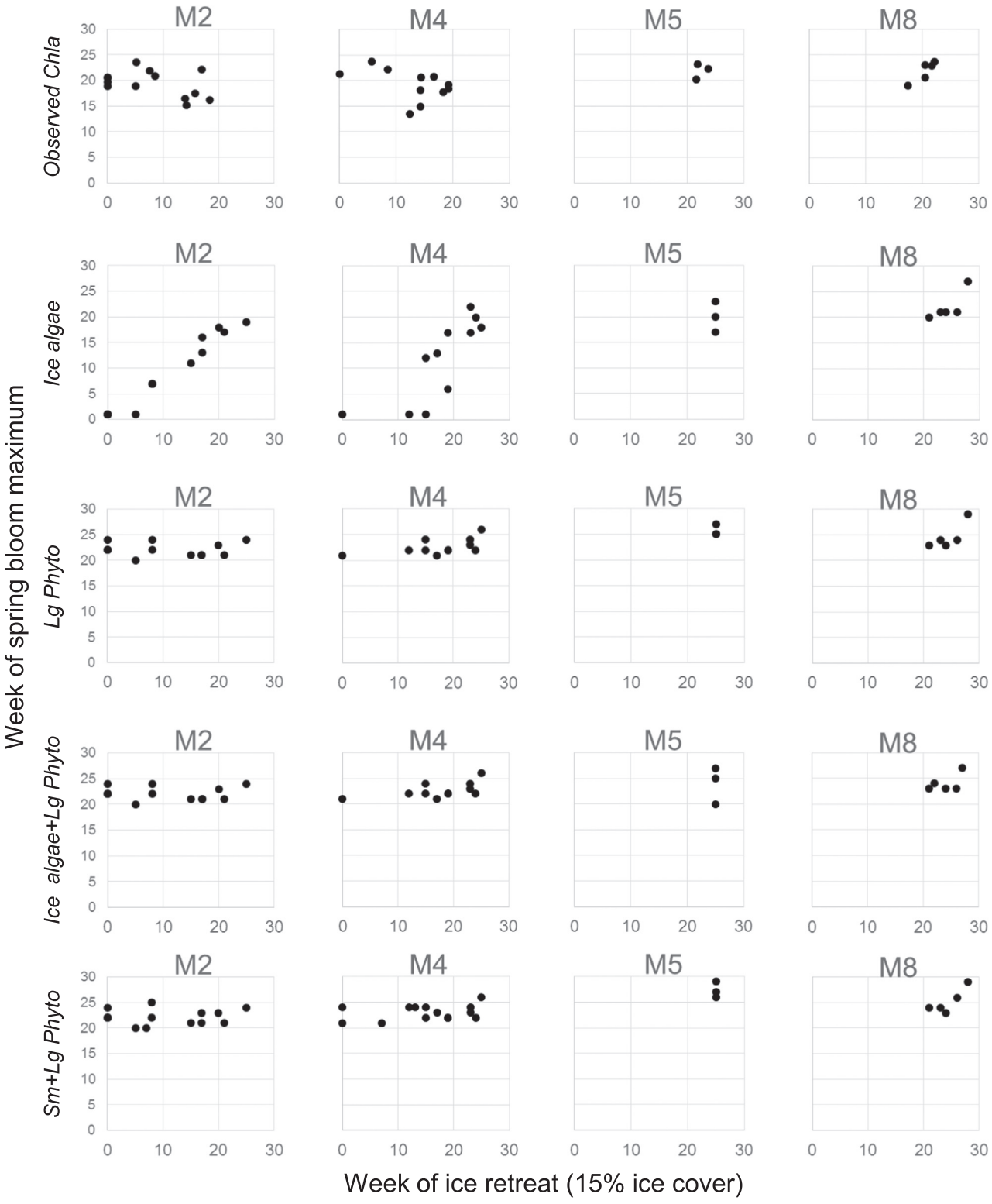

Fig. 7. Scatterplot of timing of spring bloom maximum (Julian week) and timing of ice retreat (Julian week when ice cover fell below 15%) from observed data for Chl*a* (Sigler et al., 2014) (1st row) and as estimated by the Bering10K-ROMS-BESTNPZ-FEAST model for the period 1996–2009: ice algae only (row 2), large phytoplankton biomass only (row 3), ice algae+large phytoplankton (row 4), large+small phytoplankton biomass (bottom row). Ice algae is the only variable to respond to timing of ice retreat at each mooring site and is overridden by large phytoplankton.

phytoplankton (row 4), and the sum of small and large phytoplankton (row 5). The timing of the maximum spring phytoplankton biomass was related to the timing of ice retreat at M8 and M5, regardless of which primary producers were included in the calculation (note only years with Chl*a* measurements from Sigler et al. (2014), were plotted, but when all modeled years 1996–2009 were considered, the pattern holds). Only the timing of maximum ice algae biomass responded to the timing of the ice retreat in the model at all moorings, including M2 and M4; none of the other combinations of primary producer biomass showed a

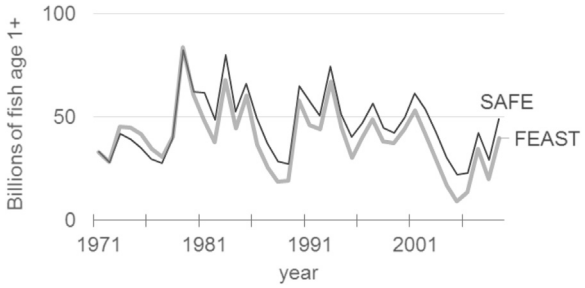

Fig. 8. Time series of number of pollock age-1 and older (1971–2009) as estimated in the EBS stock assessment model (black, SAFE) and projected using the FEAST model (gray). Number of age-1 fish calculated by FEAST were corrected to those estimated by the stock assessment at the beginning of every year.

response in their timing to that of the ice retreat. In one out of three cases the timing of the peak small+large phytoplankton biomass was later than that of large phytoplankton alone. This suggests that ice algae biomass (or ice-related primary producers) can influence the onset of spring bloom if sea ice is present. The data used in Sigler et al. (2014, appendix) show that in the south, where sea ice may or may not be present, the timing of the spring bloom can be either driven by ice-related blooms overlapping with open-water blooms or there can be an interval between an ice-related bloom and open water bloom, or in the absence of sea ice, there are only open water blooms and their timing is delayed until late spring. This validates the inclusion of ice-related primary producers included in the model, albeit their role needs to be tuned so that their biomass or dynamics within the model can indeed shift the timing of the spring bloom to an earlier date when late there is late ice retreat. Another mechanism preventing a shift to an earlier spring bloom in the model are the small phytoplankton, which might be increasing too fast in late spring and their high biomass is shifting the maximum biomass of total phytoplankton later in the year. More studies on the community composition of primary and secondary producers during late winter and early spring are needed to elucidate the extent to which ice-related plankton communities differ from or interact with late spring communities, their role in nutrient depletion and the food availability for copepods and euphausiids as they come out of diapause and overwintering.

3.1.4. Number of pollock

The number of pollock, age-1 and older, at the start of the calendar year is calculated by the FEAST model and from the stock assessment (Fig. 8). Age-1 fish in the FEAST model are corrected at the start of the year to match those from the stock assessment (Ianelli et al., 2011), while the numbers of fish from the older ages are a result of survival as calculated in the model. In general, the FEAST model calculates a slightly lower number of total fish as compared to the stock assessment (Ianelli et al., 2011). The difference appears to be due to a higher mortality on incoming age-1 (now age-2) pollock in FEAST model as well as higher fishing mortality on fish >50 cm. The first is partly due to the limited number of zooplankton over winter in the model, to which pollock respond with an increase in cannibalism and starvation. While this has been observed (see results for pollock stomach samples in Section 3.2.5), the effect is exacerbated in the FEAST model. In addition, studies by Heintz et al. (2013) have shown that low lipid storage at the start of winter is an important factor that determines the survival of age-1 pollock. Whether this was a primary factor driving the lower recruitment observed in the model (as compared to stock assessment estimates) was not quantified. The bioenergetics and population structure are set-up such that these and other relationships such as zooplankton impacts on

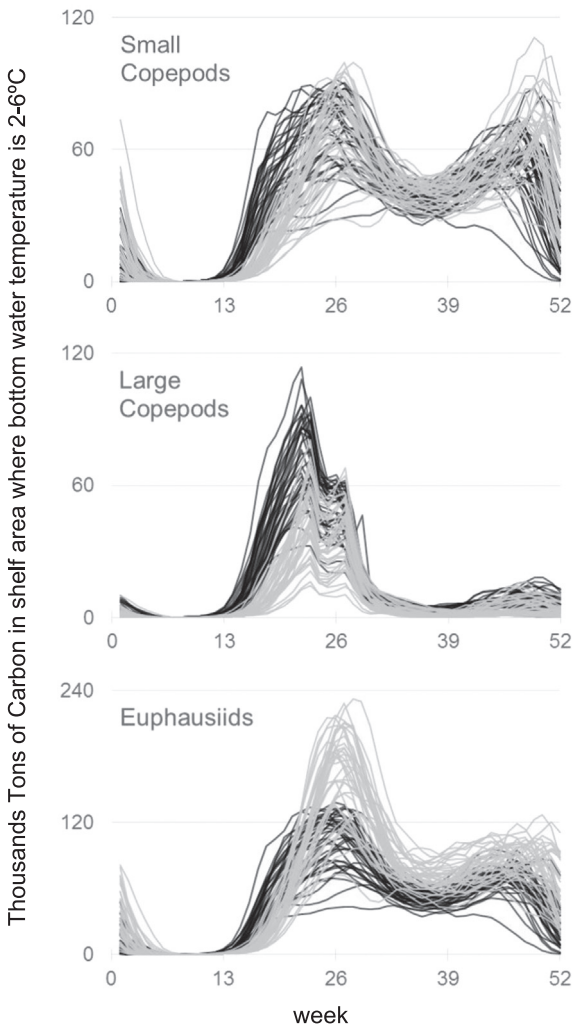

Fig. 9. Modeled zooplankton biomass in shelf areas with 2–6 °C bottom temperature range with weekly values from 1971–2009 for small copepods (top), large copepods (center), and euphausiids (bottom). Black lines show biomass as modeled by the BERING10K-ROMS-BESTNPZ model where zooplankton total mortality is based on a quadratic function resulting in mortality proportional to biomass. Light gray lines show biomass as modeled by the BERING10K-ROMS-BESTNPZ-FEAST model where zooplankton total mortality is due to both fish predation as calculated by the FEAST model and "other natural zooplankton mortality" (a reduced quadratic mortality function). Note scale for euphausiids is different.

recruitment to age-3 (Eisner et al., 2014) would be emergent properties in the model. The higher fishing mortality is due to a lower weight-at-length in the model compared to that observed in the fisheries, which leads to an overestimate of the absolute number of fish removed when converted from catch in tons.

3.1.5. Effect of fish predation on modeled seasonal zooplankton biomass (difference between one-way and two-way feedback between NPZ-FEAST)

Pollock is the main consumer of euphausiid and large copepod biomass. Fig. 9 shows the weekly biomass in shelf areas within a 2 to 6 °C temperature range for small and large copepods and euphausiids for 1971-2009, as predicted by the Bering10K-ROMS-BESTNPZ-FEAST model with one- and two-way coupling (as described in Section 2.2). With one-way coupling, the temperature-dependent quadratic mortality in the BESTNPZ model is a closure term that assumes total mortality is proportional to biomass year round. In contrast, the model configuration with two-way coupling has zooplankton mortality due to fish predation (as simulated using the FEAST model), and "other natural mortality" as simulated by a

reduced quadratic term. Including the modeled fish predation on the zooplankton dynamics captures the varying demand of zooplankton as prey by fish as a function of: predator length structure; location; increased metabolism; and relative availability of other prey. While the exact dominant mechanism is harder to isolate, in aggregate, the above factors provide the model with a varied suite of mechanisms to capture interannual and seasonal variability. The biomass of small copepods (Fig. 9, top panel), as calculated using dynamic fish predation, is lower throughout spring and early summer compared to the biomass calculated using quadratic mortality only. This is because small copepods are consumed quickly by small fish, particularly by small pollock, and it is not until fish have increased in length that other prey become available. A similar pattern is true for large copepods (Fig. 9, middle panel). The lower large copepod biomass calculated with two-way compared to one-way feedback reflects the higher consumption of copepods by fish during the spring and summer when they are most available. The demand for large copepods extends until late summer, as fish increasing in length feed less on small copepods and more on large ones. The higher consumption of copepods using two-way feedback releases the predation mortality on euphausiids, which then maintain a higher biomass throughout fall (Fig. 9 bottom panel) before overwintering. In the NPZ model, the zooplankton biomass is set to decrease until it is almost nil, so there are no overwintering euphausiids nor movement off-shelf of the large copepods. There is, however, a fixed date for start and end of diapause. When the zooplankton biomass of the various groups is shown for all areas across a thermal envelope (2–6 °C), it indicates that there can be a top-down control on zooplankton via predation by fish. The fish predation on the different zooplankton groups varies annually and depends on the time of year. The model keeps track of biomass in grams of carbon only, meaning it cannot capture changes in energetic content, and does not allow for multiple generations of euphausiids (documented for *T. longipes* in other areas [Iguchi and Ikeda, 2004] and for *T. inermis* in the Barents Sea [Dalpadado and Skojdal, 1996]). In addition, the model does not take length of euphausiids into account so a change in biomass can be interpreted as either a change in individual weight or a change in the number of individuals. Any of these factors, however, would probably only

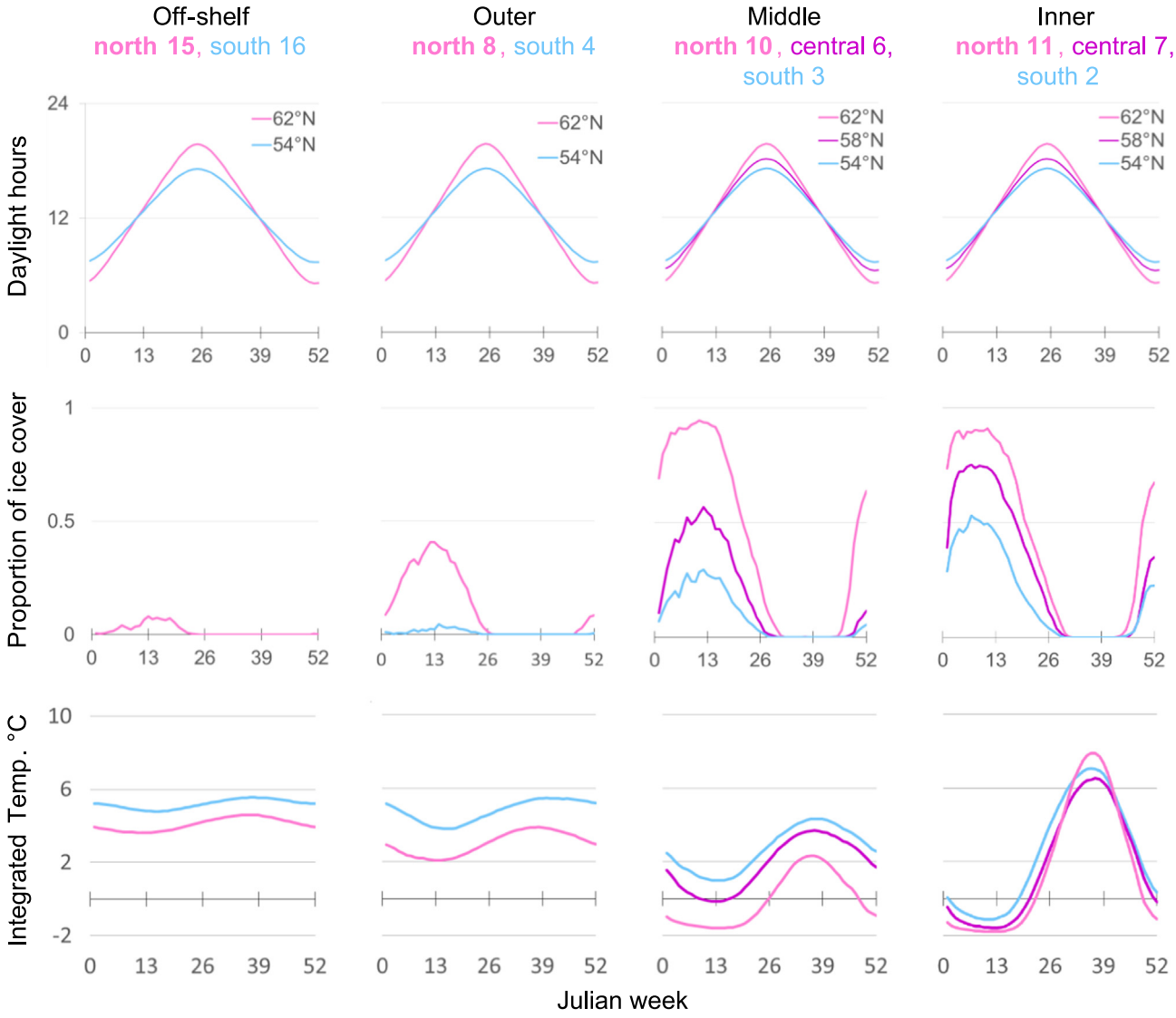

Fig. 10. Modeled physical characteristics across Bering Sea shelf and slope: Top row: weekly length of day in hours, N-S variation at 62°N, 58°N and 54°N; second row: weekly climatology of proportion of ice cover; and third row: weekly climatology of integrated temperature in °C (depth averaged temperature). Results shown for selected regions located along the cross-shelf gradient (from left to right: off-shelf, outer, middle and inner shelf) and latitudinal gradient (south, central and northern; number indicates region). Model results are averages over years 1971–2009.

slightly modify the difference in weekly biomass computed using the different coupling modes.

3.2. Climatologies by region

Here we focus first on the weekly climatologies based on model output for physical characteristics, primary producers, secondary producers and the 1971–2009 time series of euphausiid biomass and temperature. We then present the monthly and seasonal climatologies of pollock prey based on stomach samples.

3.2.1. Physical characteristics

Fig. 10 shows the off-shelf to inner shelf and latitudinal gradient across selected regions for duration of daylight, fraction of sea-ice cover and integrated water temperature in the upper 300 m or throughout the water column, whichever is shallower. The duration of daylight is shown as a guide: spring equinox,

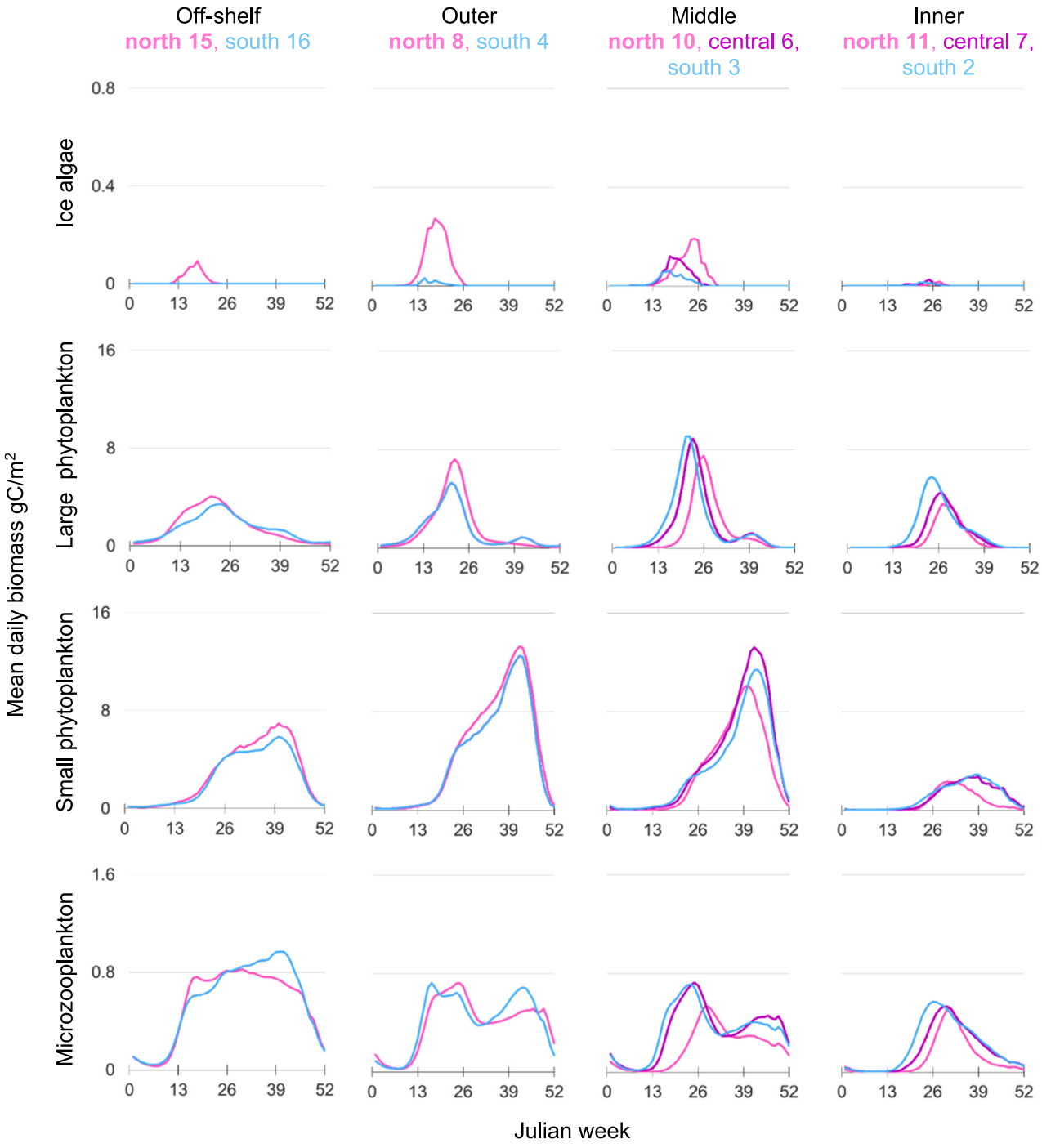

Fig. 11. Primary producers and microzooplankton across Bering Sea shelf and slope: Plots show weekly climatology of daily total biomass (gC/m^2) in the water column (max. 300 m depth), at selected regions located along a cross-shelf gradient (from left to right: off-shelf, outer, middle and inner shelf) and latitudinal gradient (south (blue), central (purple) and northern (pink)); number indicates region. Top row: ice algae; second row: large phytoplankton; third row: small phytoplankton; and bottom row: microzooplankton. Model results are computed over years 1971–2009. Note ice algae and microzooplankton have different scales. Model results are averages over years 1971–2009. (For interpretation of the references to color in this figure legend, the reader is referred to the web version of this article.)

week 12; summer solstice, week 26; fall equinox, week 38; and winter solstice, week 51. Duration of daylight only varies by latitude, so the graphs are repeated from off-shelf to the inner shelf. The fraction of ice cover increases from off-shelf to inner shelf. A strong seasonal signal exists where the average duration of ice-free waters can be as short as thirteen weeks in the north inner shelf (region 11) to near year round in the south, off-shelf (region 16). Fig. 10 (middle panels) shows the progression of ice cover, from north to south and inner to off-shelf. Sea-ice retreat is slower in the model than in the observations, so the duration of the ice-free season is underestimated over the middle shelf regions (see Section 3.1.1). However, except for the timing, the north to south pattern and relative magnitude of ice cover in the middle domain is very similar to that described by Stabeno et al. (2012a, see their Fig. 2) for moorings M2, M4, M5 and M8 along the middle shelf for the period 1972–2010. The amount of sea ice in each shelf domain is controlled by different mechanisms: primarily advection forced by winds in the south middle shelf and melting; local production in the inner shelf in areas such as Bristol Bay (region 2) and near Norton Sound (region 11), and primarily formed and melting in the north (e.g. region 10) (Stabeno et al., 2007). The integrated ocean temperature shows relatively small seasonal variation in the mostly ice-free off-shelf region, where water remains stratified even during winter (Stabeno, et al., 1998; Overland. et al., 1999). Increasingly higher seasonal variability is seen towards the inner shelf (Fig. 10, bottom row). The inner shelf is shallow (<50 m), and there is thorough mixing of the water column (Overland. et al., 1999; Sullivan et al., 2014). The largest latitudinal difference appears to be along the middle shelf, where depth-integrated temperature typically falls below 0 °C in the north, yet remains above 1 °C in the south. Lauth and Kotwicki (2013) found a bottom temperature of 1 °C to be a thermal limit for most groundfish of commercial importance on the Bering shelf. The seasonal changes in integrated temperature shown here suggest the inner shelf might be too cold for several groundfishes to overwinter in that area, and fish, including some sizes of pollock (see Fig. 2 in Buckley et al., 2016), would probably move towards the outer shelf as winter sets in. The seasonal extent of the sea ice and colder temperature concentrates pollock towards the outer shelf in winter and influences the extent of their spawning grounds, which Petrik et al. (2015) found to influence the distribution of early life stages of pollock in the EBS and potentially their spatial overlap with predators.

3.2.2. Primary producers and microzooplankton

Weekly climatologies for modeled ice algae, large phytoplankton, small phytoplankton, and microzooplankton are shown in Fig. 11 for selected regions across off-shelf to inner shelf and latitudinal gradients. The biomass values represent the vertically integrated values in the upper 300 m or entire water column, whichever is shallowest. The slower ice retreat and earlier onset of sea ice in the model compared to observations compresses the ice free period and delays the ice algae and spring bloom. However, the results are relevant in that they show the relative timing over cross-shelf and latitudinal gradients. Depending on year-specific conditions, ice algae can start the primary productivity cycle, which in turn influences the start of secondary production. Except for the delayed onset, the climatology of ice algae from the model output follow the general dynamics of ice-related blooms as described by Brown and Arrigo (2013). The model shows higher ice algae biomass in the northern and outer ice-edge areas (Fig. 11), in part because these areas have a higher and more prolonged ice cover (Fig. 10). In the middle shelf, ice algae typically start at the southern ice edge as ice retreats, in early spring (region 3), and peak in late spring north of St. Matthew Island (region 10).

We focus on the relative timing of large phytoplankton as opposed to the absolute magnitude of the maximum biomass during spring blooms. The delay of the timing of the spring bloom maximum biomass in the model (discussed in Sections 3.1.2 and 3.1.3) is also evident in the weekly climatologies across regions. The relative magnitude of the spring phytoplankton biomass across the southern shelf follows the pattern described by Rho and Whitledge (2007) and that of Lomas et al. (2012) estimated using a vertically generalized, productivity model – the highest primary production occurs in the middle shelf, decreasing towards the slope, with similar or lower values observed in the inner and outer shelves. In the northern shelf, the modeled spring phytoplankton biomass is lower for the inner than the outer shelf. The spring bloom starts off in the southern middle shelf and progresses to off-shelf and inner shelf regions in agreement with satellite images for March, April and May (Hunt et al., 2010), with the timing of the spring bloom in the inner northern shelf regions occurring six weeks later on average. In the model, high large phytoplankton biomass typically lasts for approximately three months. Small phytoplankton begin to bloom several weeks after large phytoplankton. Small and large phytoplankton peak closer in time in the northern and inner regions than in southern regions, with less pronounced summer lows and slower decrease of phytoplankton biomass towards the end of fall (see observed Chl*a* at M8, Fig. 6). This decreasing pattern is not captured for the northern regions in the model; only the closer timing of the spring and fall bloom is captured. As mentioned earlier, the model overestimates the biomass of small phytoplankton which drives the fall bloom, and in turn may extend the growth period of zooplankton. This overestimation of the fall bloom is systematic across the slope and shelf areas as compared to domain-based estimates shown by Hunt et al. (2010), and when considering their contribution to total Chl*a* biomass. In late summer (August and September), small phytoplankton usually make up 10% to 50% of total Chl*a* biomass across the entire shelf and around 20% in the outer shelf (Eisner et al., 2016, Fig. 6 in their paper). Both large and small phytoplankton appear to fuel microzooplankton (bottom panel, Fig. 11). Since the large and small phytoplankton blooms are typically separated by a drop in biomass in early summer, regionally coherent patterns emerge despite the lagged timing in the model and the interannual variability in the magnitude of the peak biomasses and the different physical processes driving the dynamics in the northern versus southern, and inner versus outer shelves (Stabeno et al., 2012a). The different spatial scales of the environmental variability of factors, such as the timing of ice retreat, vertical stratification and mixing across regions, means local conditions are not uniformly favorable or unfavorable across the shelf and slope, and biological responses may vary between regions while still having spatial coherence, as shown by Eisner et al. (2016), see their Table 2). This applies to both differences between the north and the south, which have uncorrelated warm/cold years (Stabeno et al., 2012b; Luchin and Panteleev, 2014) and within the north and the south, as cross-shelf differences such as bathymetry and tidal currents buffer or intensify the impact of environmental factors.

3.2.3. Secondary producers

The spatial coherence and timing sequence is evident in the 1971–2009 mean weekly biomass for the small copepods and euphausiids (Fig. 12). The peak biomass of small copepods is shortly followed by an increase in the biomass of large copepods and euphausiids. As with phytoplankton, these increases occur later in the model than the observations, but in both progresses towards the northernmost and inner shelf regions. Model estimates here have several biases. In addition to the overall delay in the reproductive/growth cycle, large copepods are probably

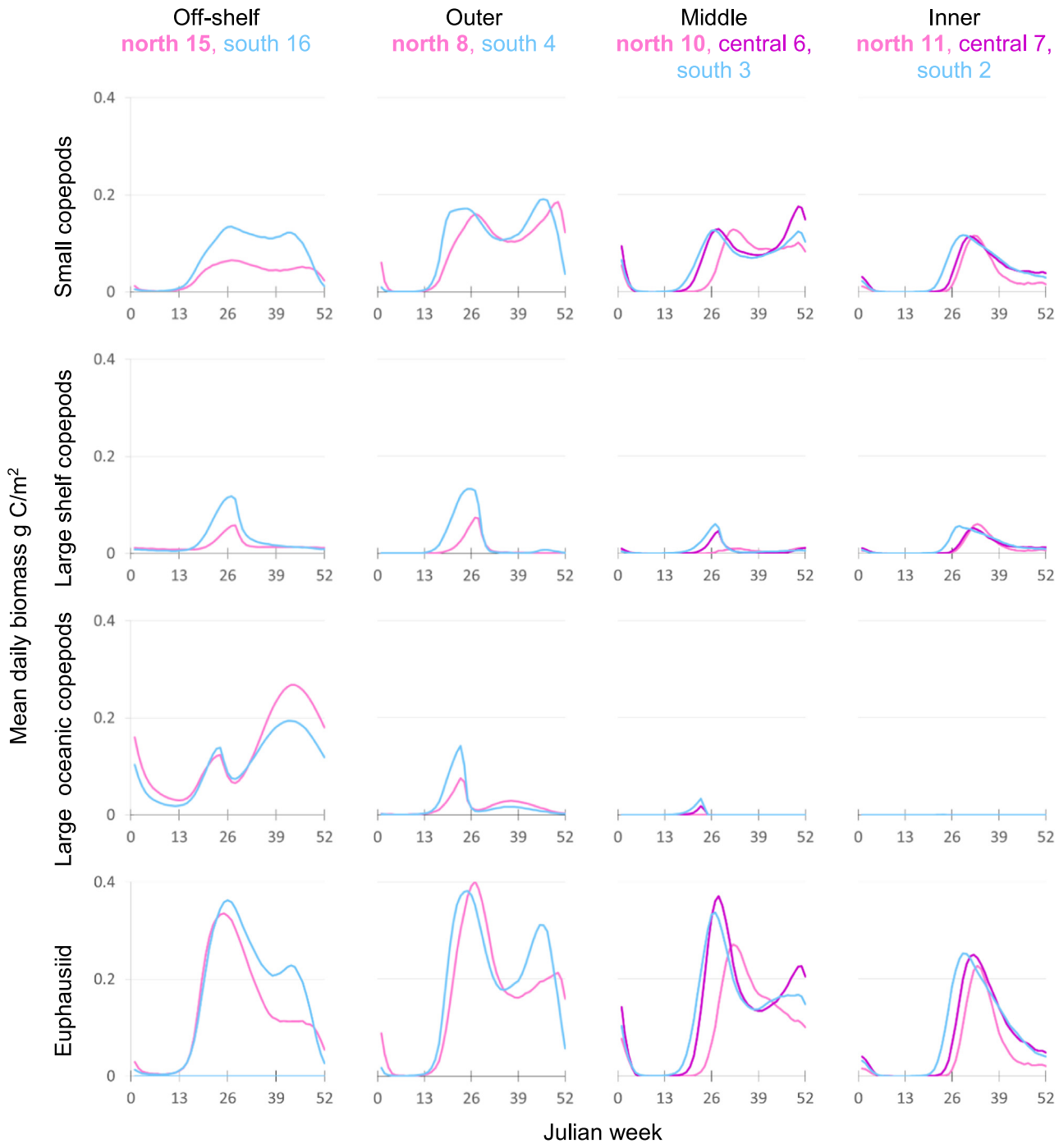

Fig. 12. Secondary producers across Bering Sea shelf and slope: Plots show weekly climatology of daily total biomass (gC/m^2) in water column (max. 300 m depth), at selected regions located along the cross-shelf gradient (from left to right: off-shelf, outer, middle and inner shelf) and latitudinal gradient (south (blue), central (purple) and northern (pink)); number indicates region. Top row: small copepods; second row: large shelf copepods; third row: large oceanic copepods, and bottom row: euphausiids. Model results are averages over years 1971–2009. (For interpretation of the references to color in this figure legend,the reader is referred to the web version of this article.)

underestimated in magnitude and seasonal availability. The seasonal availability is shortened on both ends: the delayed reproduction/growing cycle due to the delayed timing of the spring blooms and the early diapause imposed by a fixed start date; each attenuate dynamic responses to favorable environmental conditions. Copepod biomass has been observed to peak in fall (Eisner et al., 2014), but this is not possible in the model set-up used here. A revised version of the NPZ model is currently being evaluated using alternative set-ups. A better understanding of the mechanisms driving the onset or termination of copepods diapause and quantitative relationships between environmental factors and diapause timing would also improve future models. The large oceanic copepod biomass in the offshore area increases after diapause. This increase in biomass is likely a model artifact and not something that occurs in reality, as: i) it is coming entirely from deep-water layers, where small concentrations of copepods are magnified by the integrated sum due to the expanding thickness of the deep layers; and ii) no other zooplankton groups show corresponding trends (see Fig. 12, first column). The earlier timing of the increase in euphausiid biomass in the model output for the outer shelf and off-shelf areas resembles that of the dominant species in the outer shelf, *Thysanoessa inermis*, which spawns in

April. Likewise, the later biomass increase in the middle shelf would be akin to spawning of *T. raschii*, which occurs mid- to late-May (Vidal and Smith, 1986; Smith, 1991) and may extend to at least August, when collected individuals had spermatophores, indicating they were breeding (Hunt et al., 1996). The fall increase in the biomass of small copepods and euphausiids in the model output seems to be driven, at least partially, by the fall phytoplankton bloom. However, we did not quantify the relative contribution of microzooplankton versus phytoplankton to the biomass increase of either small copepods or euphausiids.

The increase in both phytoplankton and zooplankton biomass in the fall is evidence that sufficiently favorable conditions may occur to support large fall blooms, albeit their frequency is overestimated in this model. Mid- to late-fall increases in plankton biomass can be highly important for the ecosystem as they would allow for a longer period of lipid storage for young pollock (Heintz et al., 2013), can favor a longer growing season for copepods (Morata and Søreide, 2015) and lipid storage for both copepods (Tsuda et al., 2001) and euphausiids (Harvey et al., 2012). However, few data exist for this time of year because most surveys end by early fall (Eisner et al., 2014, 2016). The importance of euphausiids as prey for pollock over the late fall and winter cannot be overstated, and a longer growing and lipid storage season would translate into higher quality prey.

3.2.4. *Variability in euphausiid biomass by region*

Because of the importance of euphausiids as year-round prey for pollock, we show the entire 1971-2009 time series of weekly anomalies of integrated temperature and euphausiid biomass for selected regions in Fig. 13. The model assumes river runoff is the same temperature as the receiving oceanic waters. However, rivers may discharge warm water, as is the case of the Yukon River (Dean et al., 1989). In Fig. 13, the inner shelf is shown at the top transitioning to off-shelf at the bottom. Within each shelf domain, we show time series for a region in the north and one in the south, top to bottom. Results from a hindcast simulated with a previous version of the Bering10K-ROMS-BESTNPZ model (Hermann et al., 2013) found that large crustaceans (*Neocalanus* and euphausiids) tended to covary inversely to temperature on the outer shelf. A more rigorous analysis of the observed temperature and euphausiid biomass as estimated by acoustic surveys was conducted by Ressler et al. (2014), but others have also made similar observations from field data (Hunt et al., 2011; Coyle et al., 2011). Inverse covariance between large crustacean abundance and temperature appears to be stronger during the recent string of warm (2001-2005) and cold years (2007–2013) than during the earlier years, but is particularly evident in off-shelf/slope areas (regions 15 and 16 in Fig. 13). Years prior to 1977 had a weaker inverse covariance, and Hermann et al. (2013) reported a positive correlation between temperature and large crustacean zooplankton on the inner and northern shelf. This tendency in the north and inner areas may be linked to changes in the dominant water mass and to flow reversals due to wind-driven currents (Danielson et al., 2012). In the inner domain, the temperature anomalies show higher variability, disrupting what would be a multi-year monotonic trend in other areas and highlighting the differences in timing and magnitude of warm/cold years in the north compared to the south shelf. While this might be influenced by the dominant water masses, the main factor is likely the timing of ice retreat and river runoff. We did not conduct any analysis to evaluate whether it is current variability that interrupts the monotonic trend observed elsewhere. Another off-shelf to inner shelf gradient in the physics (which affects the zooplankton), is the higher frequency interannual variability towards the inner shelf, with lower frequency variability towards the off-shelf areas. A spectral analysis conducted by Hermann et al. (t2016, Figs. 18 and 19 in their paper) confirms 1–2 year interannual variability in the inner shelf (top portion Fig. 13), while interannual variability is characterized by processes of typically 2–4 years frequency in the off-shelf (lower portion Fig.13). This partly explains why the off-shelf area is much more stable year-round than the inner shelf. Other processes influencing the frequency of the variability include: ice expansion and retreat over the shelf, but lacking in the basin; strong advection in the outer shelf that removes the ice signal; and winds in shallow areas

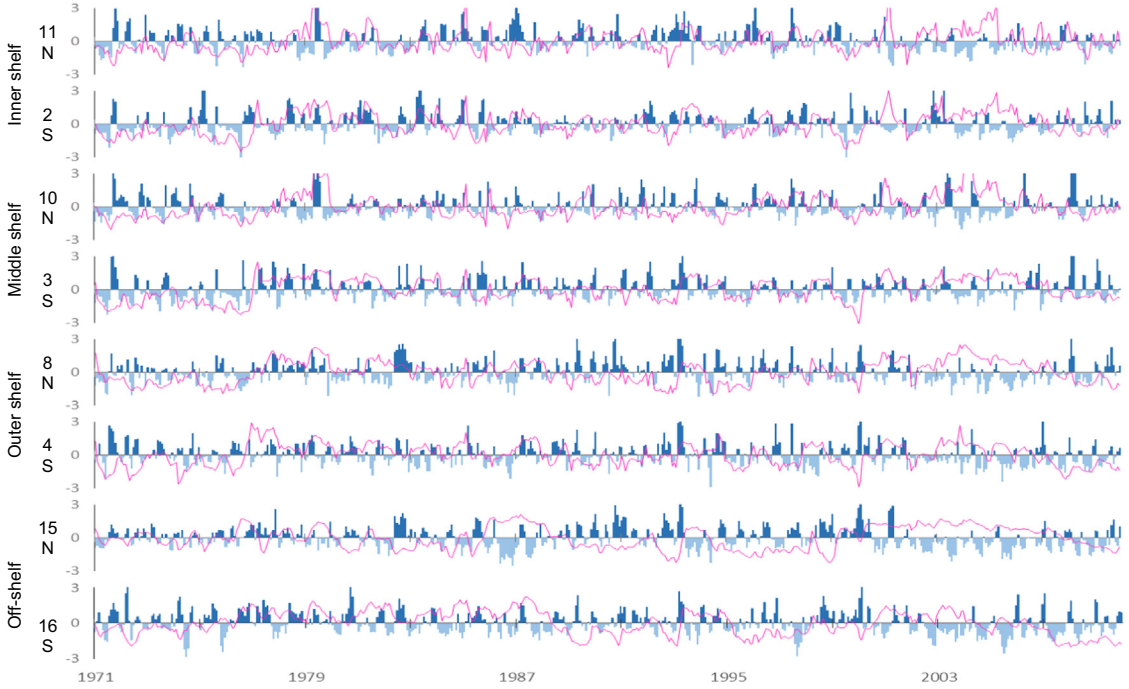

Fig. 13. Weekly anomalies of euphausiid biomass (mgCm^2, bars) and depth-averaged temperature anomaly (red line) at selected regions from 1971–2009. Top to bottom: inner, middle, outer and off-shelf; north (upper) and south (lower) regions are shown for each shelf domain. See Section 3.2.4 for details. (For interpretation of the references to color in this figure legend,the reader is referred to the web version of this article.)

which can mix the entire water column, while in the off-shelf, winds mix only the upper water column (above 20 m) and the water column remains stratified throughout the year (Stabeno et al., 1998).

3.2.5. Euphausiids, copepods and pollock as prey of pollock

Pollock diet data for fish 8 mm – 80 mm collected over 30 years are summarized for selected regions (n = 58,403) in Fig. 14. The monthly frequency of occurrence of euphausiids, copepods and pollock in pollock stomachs show copepods have a strong seasonal availability (primarily spring and summer), while euphausiids remain an important prey throughout most of the year, with a possible peak in late fall as well as in the spring (Fig. 14, 1st column; see also Buckley et al. (2016) for complete prey composition by length and area). This is likely due to their continued availability: while copepods go into diapause and remain near the bottom (Baier and Napp, 2003), euphausiids overwinter; they have a restricted vertical migration and may also switch to detrital and benthic feeding (Sargent and Falk-Petersen, 1981; Huenerlage et al., 2015), making them accessible to pollock as part of the hyperbenthos. In any given year, the available euphausiid biomass is the result not only of the reproduction and growth of the year's cohort, but is likely multi-generational (Dalpadado and Skojdal, 1996). Interannual patterns also indicate that during the summers when copepods are less available, pollock do not increase their consumption of euphausiids (Buckley et al., 2016). The importance of copepods to summer feeding success, and pollock size-related patterns in summer feeding migration relative to geographic distributions of copepods and euphausiids (Buckley et al., 2016) explains why pollock biomass is not a reliable predictor of euphausiid abundance and why pollock predation on euphausiids does not necessarily result in top down control, as noted by Ressler et al. (2014). However, Hunt et al. (2016) noted a strong negative relationship between euphausiid biomass and pollock biomass.

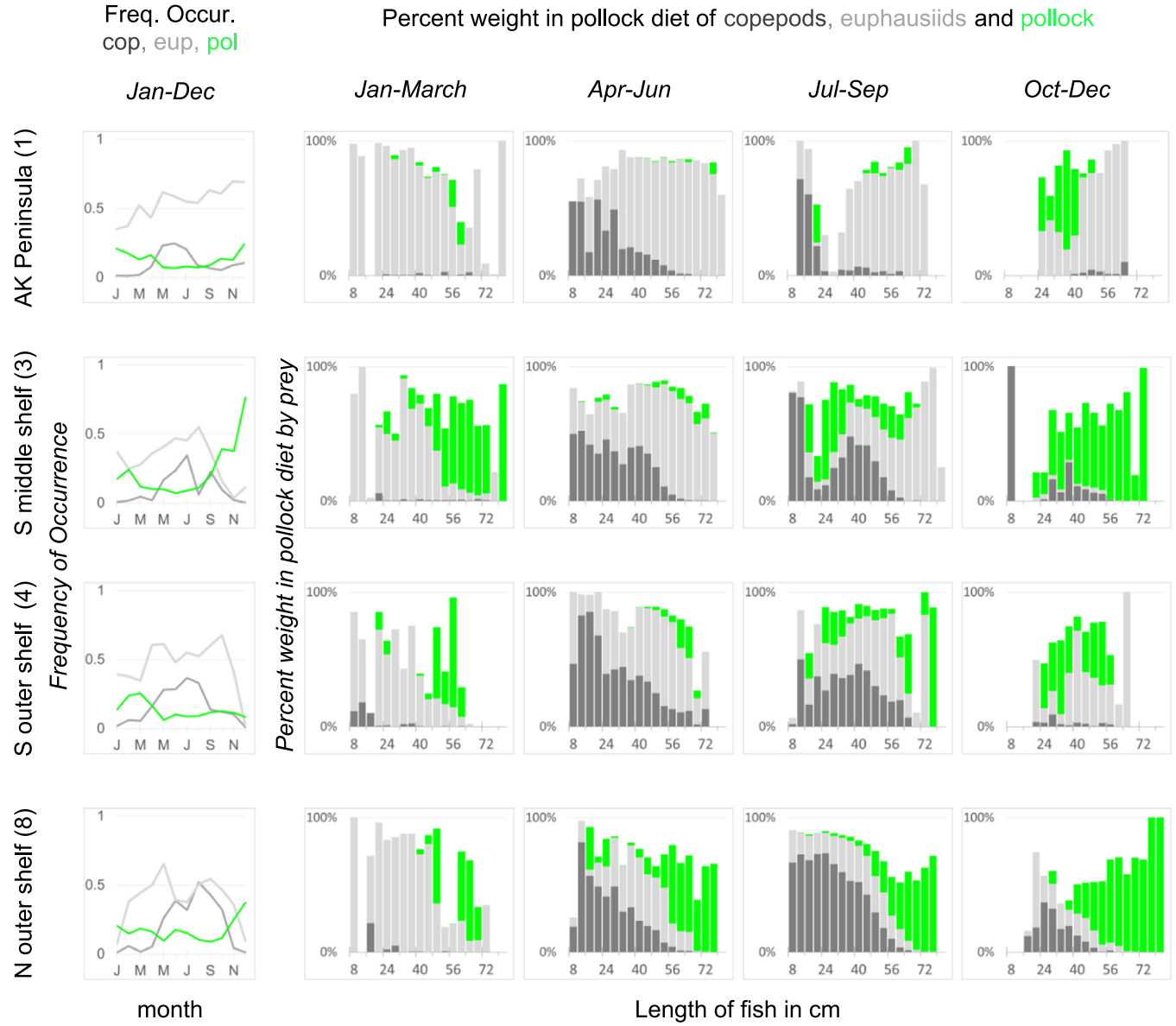

Fig. 14. Copepods, euphausiids and pollock in pollock stomachs: Plots show monthly frequency of occurrence (first column), and seasonal percent weight in diet by length of fish in cm (columns 2–5) for copepods (dark gray), euphausiids (light gray) and pollock (green). Results are shown for stomachs collected at selected regions: Top row region 1 (north of AK peninsula), region 3 (middle south shelf), region 4 (south outer shelf) and region 8 (north outer shelf). Stomachs were collected year-round, on surveys and by observers, between 1982 and 2013. BSIERP domains 1, 3, 4, and 8 have 31 years of pollock diet data. Samples include all non-empty pollock stomachs. (For interpretation of the references to color in this figure legend, the reader is referred to the web version of this article.)

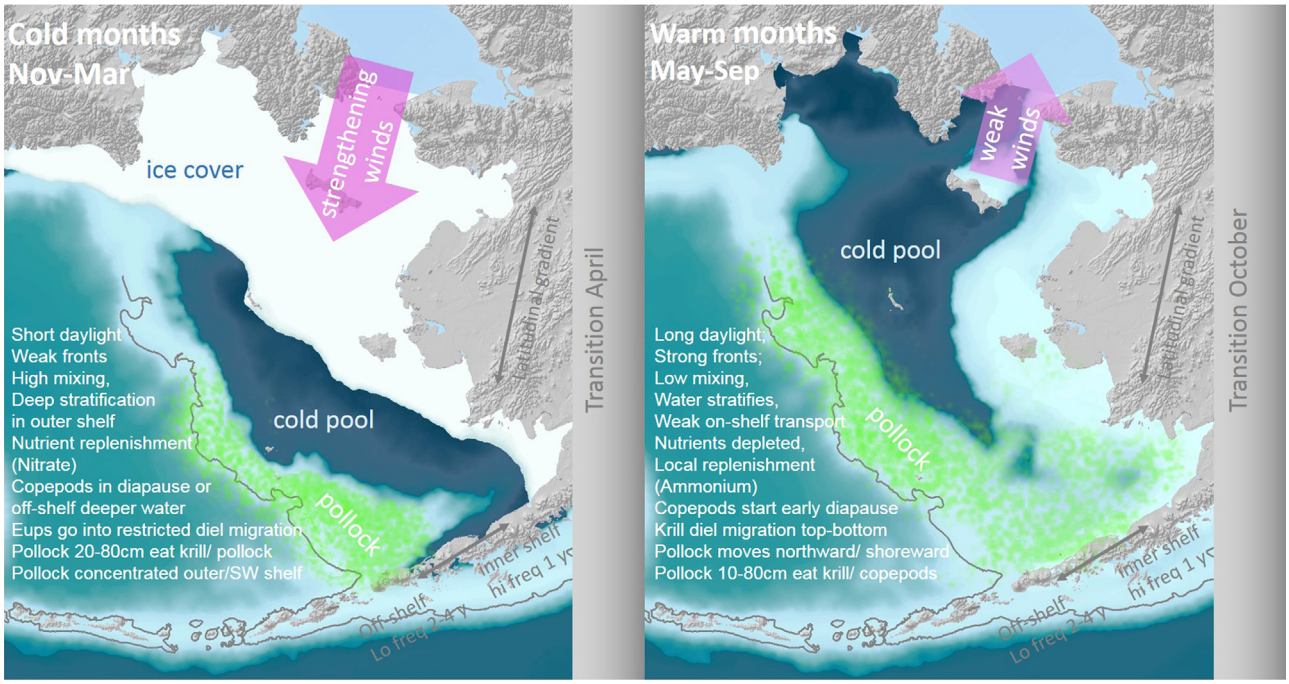

Fig. 15. Seasonal synthesis of physical and biological processes in the eastern Bering Sea shelf and slope.

More studies are needed to evaluate the relative abundance of copepods with respect to euphausiids and how top-down control of euphausiids by pollock may be attenuated by relative availability of copepods as prey and other factors. The decreased availability of copepods is at least partly substituted by the increased cannibalism during late fall and early winter. The occurrence and the amount of cannibalism is highest where the distribution of large and small pollock overlap (Boldt et al., 2012, see Fig. 7 of Buckley et al., 2016 for example of distribution of pollock by length). Cannibalism by pollock is particularly high in the south middle shelf (region 3) in winter, in the outer shelf during spring and summer (region 8), and is most widespread in fall. Given the importance of fall conditions for determining pollock survival in the model, direct measurements of mid- to late-fall zooplankton could be very influential. The contribution of euphausiids, copepods and small pollock to the pollock diet is supplemented by local zooplankton communities and other larger prey. While euphausiids were not evaluated by Eisner et al. (2014) since sample collection was conducted during daylight when euphausiids were located too close to the sea floor to sample quantitatively, their results show *Calanus* spp. were in higher abundances in middle and outer shelf regions than in the inner shelf during August to September. These taxa are responsible for most of the large copepod biomass, which matches the presence of large copepods in diets of pollock greater than 20 cm. Likewise, mysids and shrimp in the southeastern Bering Sea were in highest concentrations in the inner shelf, which seems to match with diet data (although shrimp are also present in diets elsewhere on the shelf) (Buckley et al., 2016).

4. Summary and conclusion

Understanding the processes that lead to spatiotemporal variability in the flow of energy from primary production through successive trophic levels is key to predicting potential effects of climate change on upper trophic levels and commercially important species. While overall trends in primary and secondary production are indeed relevant as indicators of maximum energy available for transfer in the system, it may be that pockets of high prey abundances or more suitable temperatures provide a spatial energetic refuge for forage and upper trophic levels. Our results are in agreement with Buckley et al. (2016), showing that pollock might feed on copepods more and on euphausiids less than previously believed (Ressler et al., 2012). If so, the succession of zooplankton blooms and length of availability of copepod versus euphausiid prey (growing season versus year-round, respectively) might be equally influential in driving pollock survival and/or distribution, than considering only their abundance. The seasonal and interannual availability of necessary resources – or the lack thereof – contributes to the success or failure of particular age classes or reproductive seasons.

As flows of available prey and energy vary seasonally, it is important to understand how and when these resources become available to upper trophic levels, and the role of their location within the water column. For example, vertical, horizontal and temporal distribution are important mechanisms for niche partitioning, allowing for spatial overlaps or mismatches, not only for fish and zooplankton, but also seabirds and whales (Russel et al., 1999; Harvey et al., 2009; Hunt et al., 2014; Siddon et al., 2013; Sigler et al., 2014). Because of the implications that climate variability may have on primary and secondary production, it is important to understand driving factors prone to change – such as temperature, sea-ice cover timing and duration, winds and currents – and distinguish them from those that will keep their current pattern such as length of day, bathymetry, and tidal currents. For example, vertical mixing in shallow (<30 m) areas is primarily influenced by tidal mixing whereas in the middle and outer shelf where tidal currents are weaker, wind-driven mixing and thermal stratification play a major role. Hence vertical mixing in the middle and outer shelf is potentially more susceptible to climate change than in shallow areas. Similarly, tidal currents are three times stronger in the southern than in the northern Bering Sea shelf (Stabeno et al., 2012a), meaning the northern shallow areas may be more susceptible to future changes in vertical mixing than those in the south. Assuming northward winds and temperature will increase in the future, the position of the middle front would be more susceptible to change than that of the inner

front. Based on the forecasts by Hermann et al. (2016), preliminary analyses show that the spring bloom, which is driven by physical changes, may shift to an earlier time in the north, and to a later time in the south.

The spatiotemporal patterns of the physical and biological characteristics addressed in this paper are emergent properties of the model. We use its general coherence with observed patterns as a basis to synthesize processes in the EBS shelf and slope environment, during warm and cold months (after Stabeno et al., 2016) as shown in Fig. 15. Sea-ice cover (itself driven largely by wind in the northern Bering Sea; Stabeno et al., 2007) serves as a primary driver of both bottom and pelagic habitat by creating a higher water density cold pool that serves as a thermal boundary (Lauth and Kotwicki, 2013). Both ice cover and the cold pool expand and contract seasonally (Wyllie-Echeverria and Wooster, 1998), concentrating pollock (20–59 cm long) towards the outer shelf and slope (Buckley et al., 2016; Kotwicki et al., 2005) at their maximum extent during cold months (November to March, winter and early spring). Ice cover contracts over spring months and the cold pool progressively contract northward throughout the warm months (May to September, late spring and summer). In spring as the ice melts, the ocean warms and water stratifies (Niebauer et al., 1995; Sullivan et al., 2014), and primary and secondary production (Stabeno et al., 2010) and pollock follow. Prevailing features during warm months include: a) sea-ice absence and retreat; b) stronger fronts and weaker across-shelf water exchange (Stabeno et al., 2016), higher local nutrient regeneration/recycling of nitrate (Cheng et al., 2016), (although episodic uncoupling of the nitrogen cycle can lead to nitrite accumulation, Mordy et al., 2010; c) weak variable winds (northeastward on average) over the shelf (Danielson et al., 2012); and d) warm saltier water advected northward by the Anadyr Current in the north (Coachman et al., 1975; Wang et al., 2009). During October, a transition month (early to mid-fall), depth-averaged temperature begins to decrease, and the mixed layer begins to deepen on the southeastern shelf (Sigler et al., 2014). Large-scale physical processes shift to their typical cold months (winter-early spring) features: a) advance of ice; b) weak frontal structure on the shelf (Coachman, 1986; Stabeno and Hunt, 2002) that allow cross-shelf wind driven flow, favoring nitrate replenishment in the southern shelf (Stabeno et al., 2016); c) increasingly southwestward winds over the shelf, strengthening through December (Danielson et al., 2012); d) in the north, cold salty water is advected eastward by winds (Coachman et al., 1975; Wang et al., 2009). While there is spatial coherence among contiguous regions, conditions do not vary shelf-wide in the same proportion due to the spatial variability of these large scale physical processes (Eisner et al., 2016; Luchin and Panteleev, 2014; Stabeno et al., 2016). Zooplankton and pollock are finely tuned to this system. Seasonal energetic sources for euphausiids switch from pelagic phytoplankton and zooplankton in the spring and summer to the benthos in fall and winter while copepods go into diapause (Baier and Napp, 2003). Seasonal energetic sources for pollock switch from pelagic zooplankton in the spring and summer to stored energy from lipids, overwintering euphausiids, and cannibalism in the fall and winter. The spatial progression in the timing, peaks and sequence of events throughout the shelf, as well as regional and length specific pollock diets, are coherent with a seasonal expansion and contraction of pollock distribution, and support the feeding and spawning migration routes for pollock (Buckley et al., 2016; Kotwicki et al., 2005, 2015).

Some of the most beneficial aspects of the model hindcast described here have been the syntheses it has prompted, how it has provided a year-round framework for local or seasonal observations, and how it has helped identify gaps, guiding research both in the design and temporal focus of surveys. Recent improvements to the models presented here already have a tighter link to benthic energy sources and sinks and improved ice dynamics. Other simplifications, such as no diel migration by euphausiids and no overwintering in the zooplankton dynamics, are being addressed. These modifications, as well as increasing the growing season for copepods, will impact the calculated values for movement, diets, survival and growth of pollock (and other fish) in the model. The small phytoplankton and microzooplankton biomass will likely be re-evaluated as well. As our understanding of the variability and plasticity of life history strategies within each of these multi-species groups increases, the modeling framework will evolve to incorporate the more important differentiating characteristics. Multidecadal projections such as those conducted by Hermann et al. (2016) have shown potential changes in habitat (cold pool) as perceived by groundfish. The ability to run simulations of integrated ecosystem models has proven a necessary tool to elucidate potential costs and benefits of management strategies, as well as future challenges (Fulton, 2011; Fulton et al., 2014).

Our project highlights the benefits of linking continuous and long-term field work with the development and implementation of highly complex models. Models such as these serve as tools to identify information gaps, test process hypotheses, and prioritize research. They are essential to a coordinated understanding of the linkages and responses between co-varying environmental factors, climate variability, and fish dynamics – an increasingly pressing need within resource management. In the face of uncertainty, simulations such as these tightly, coupled to field programs, will become more common as testbeds for process exploration and management evaluation, increasing their relevance for future fisheries and ecosystem management and strategic planning.

Acknowledgments

The authors would like to acknowledge the collective contribution of all the researchers involved in the Bering Sea Project who generously shared data and expertize. Ed Farley, Patrick Ressler, Mike Sigler, Cal Mordy, George Hunt, two anonymous reviewers, and the guest editor, Phyllis Stabeno, are thanked for their comments and insights on earlier versions of this paper. IO, AJH, AEP, EM and JM were partially supported by the North Pacific Research Board (NPRB) as part of the Bering Sea Integrated Ecosystem Research Program (NPRB BSIERP grants B52, B70, B71 and B73). MW, NB, WC, EC and KH, were partially supported by National Science Foundation grant number 0732534; GG was funded by NSF awards ARC-1107203 and ARC-0732538. FKW was fully supported by NPRB in his former role as Science Director and Modeling Manager for NPRB. This work was partially funded by JISAO under NOAA cooperative agreement NA100AR4320148; NSF grant: “Bering Sea Ecosystem Study” (NSF-0732534). This research is contribution No. 4286 from NOAA/Pacific Marine Environmental Laboratory, contribution EcoFOCI-0873 to NOAA's Ecosystems Fisheries-Oceanography Coordinated Investigations, publication 597 from the North Pacific Research Board; and 169 from the BEST-BSIERP Bering Sea Project. This publication is partially funded by the Joint Institute for the Study of the Atmosphere and Ocean, University of Washington, contribution No. 2016-01-19.

References

ADFG, 2011. ADF&G Groundfish/Shellfish Statistical Areas, Chart 3 – Bering Sea. 2nd Ed., March 2011. ⟨http://www.adfg.alaska.gov/static/fishing/PDFs/commercial/chart03_bs.pdf⟩.

Allen, B.M., Angliss, R.P., 2012 Alaska Marine Mammal Stock Assessment, 2012. U.S. Dept. Commer. NOAA Technical Memorandum NMFS-AFSC-245. 282 p. Downloaded 05/2013 ⟨http://www.nmfs.noaa.gov/pr/sars/pdf/ak2012.pdf⟩.

ARCUS, 2004. Bering Ecosystem Study (BEST) Science Plan. Arctic Research Consortium of the U.S, Fairbanks, AK, p. 82.
ARCUS, 2005. Bering Ecosystem Study Program (BEST) Implementation Plan. Arctic Research Consortium of the U.S, Fairbanks, AK, p. 43.
Aydin, K., Gaichas, S., Ortiz, I., Kinzey, D., Friday, N., 2007. Comparison of the Bering Sea, Gulf of Alaska, and Aleutian Islands Large Marine Ecosystems through food web modeling, NOAA Technical Memorandum NMFS-AFSC-178. ⟨http://www.afsc.noaa.gov/Publications/AFSC-TM/NOAA-TM-AFSC-178.pdf⟩
Baier, C.T., Napp, J.M., 2003. Climate-induced variability in *Calanus marshallae* populations. J. Plankton Res. 25, 771–782.
Barbeaux, S.J., 2012. Scientific acoustic data from commercial fishing vessels, eastern Bering Sea walleye pollock (*Theragrachalcogramma*) (Ph.D. Thesis). University of Washington, p. 219.
Boldt, J.L., Buckley, T.W., Rooper, C.N., Aydin, K., 2012. Factors influencing cannibalism and abundance of walleye pollock (*Theragra chalcogramma*) on the eastern Bering Sea shelf, 1982–2006. Fish. Bull. 110, 293–306.
Boyd, C., Dalton, M., Ianelli, J., Murphy, J., Punt, A.E., 2014. BSIERP: Integrate Models of Pollock and Cod. North Pacific Research Board, p. 58.
Brander, K., 2013. Climate and current anthropogenic impacts on fisheries. Clim. Change. 119, 9–21.
Brown, Z.W., Arrigo, K.R., 2013. Sea-ice impacts on spring bloom dynamics and net primary production in the eastern Bering Sea. J. Geophys. Res. 11, 1–20. http://dx.doi.org/10.1029/2012JC008034.
Brown, Z.W., van Dijken, G.L., Arrigo, K.R., 2011. A reassessment of primary production and environmental change in the Bering Sea. J. Geophys. Res. 116, C08014. http://dx.doi.org/10.1029/2010JC006766.
Buckley, T.W., Kappler, K., Ressler, P.H., Aydin, K.A., Hibpshman, R.E., Jones, D., McCarthy, A., In preparation. Comparisons of pollock diets from midwater and bottom trawl surveys, and comparisons of net-caught and pollock-consumed euphausiids in 2009 and 2010 in the EBS.
Buckley, T.W., Livingston, P.A. 1994. A bioenergetics model of walleye pollock (Theragra chalcogramma) in the Eastern Bring Sea: Structure and documentation. NOAA Technical Memorandum NMFS-AFSC-37. ⟨http://www.afsc.noaa.gov/Publications/AFSC-TM/NOAA-TM-AFSC-37.pdf⟩.
Buckley, T.W., Ortiz, I., Kotwicki, S., Aydin, K., 2016. Summer diet composition of walleye pollock and predator–prey relationships with copepods and euphausiids in the eastern Bering Sea, 1987–2011. Deep-Sea Res. II 134, 302–311. http://dx.doi.org/10.1016/j.dsr2.2015.10.009.
Carton, J.A., Giese, B.S., 2008. A reanalysis of ocean climate using Simple Ocean Data Assimilation (SODA), Mon. Wea. Rev. 136, 2999–3017.
Cheng, W., Curchitser, E., Stock, C., Hermann, A., Cokelet, E., Mordy, C., Stabeno, P., Hervieux, G., Castruccio, F., 2016. What processes contribute to the spring and fall bloom co-variability on the Eastern Bering Sea shelf? Deep-Sea Res. II 134, 128–140. http://dx.doi.org/10.1016/j.dsr2.2015.07.009.
Ciannelli, L., Brodeur, R.D., Buckley, T.W., 1998. Development and application of a bioenergetics model for juvenile walleye pollock. J. Fish. Biol. 52, 879–898.
Coachman, L.K., 1986. Circulation, water masses, and fluxes on the southern Bering Sea shelf. Cont. Shelf Res 5, 23–108.
Coachman, L.K., Aagaard, K., Tripp, R.B., 1975. Bering Strait: The Regional Physical Oceanography. University of Washington Press, Seattle, p. 172.
Coyle, K.O., Eisner, L.B., Mueter, F.J., Pinchuk, A.I., Janout, M.A., Cieciel, K.D., Farley, E. V., Andrews, A.G., 2011. Climate change in the southeastern Bering Sea: impacts on pollock stocks and implications for the oscillating control hypothesis. Fish. Ocean 20, 139–156.
Curchitser, E.N., Haidvogel, D.B., Hermann, A.J., Dobbins, E.L., Powell, T.M., Kaplan, A., 2005. Multi-scale modeling of the North Pacific Ocean: assessment and analysis of simulated basin-scale variability (1996–2003). J. Geophys. Res. 110, C11021. http://dx.doi.org/10.1029/2005JC002902.
Dalpadado, P., Skojdal, H.R., 1996. Abundance, maturity and growth of the krill species *Thysanoessa inermis* and *T. longicaudata* in the Barents Sea. Mar. Ecol. Prog. Ser. 144, 175–183.
Danielson, S., Curchitser, E., Hedstrom, K., Weingartner, T., Stabeno, P., 2011. On ocean and sea-ice modes of variability in the Bering Sea. J. Geophys. Res. 116, C12034. http://dx.doi.org/10.1029/2011JC007389.
Danielson, S., Hedstrom, K., Aagaard, K., Weingartner, T., Curchitser, E., 2012. Wind-induced reorganization of the Bering shelf circulation. Geophys. Res. Lett. 39, L08601. http://dx.doi.org/10.1029/2012GL051231.
Dean, K.G., McRoy, P., Ahlnäs, K., Springer, A., 1989. The plume of the Yukon River in relation to the oceanography of the Bering Sea. Remote Sens. Environ. 28, 75–84.
Denlinger, L.M., 2006. Alaska Seabird Information Series. Unpubl. Rept., U.S. Fish and Wildl. Serv., Migr. Bird Manage. Nongame Program, Anchorage, AK. Downloaded 05/2013. ⟨http://www.fws.gov/alaska/mbsp/mbm/seabirds/pdf/asis_complete.pdf⟩.
Eisner, L.B., Gann, J.C., Ladd, C., Cieciel, K.D., Mordy, C., 2016. Late summer/early fall phytoplankton biomass (chlorophyll a) in the eastern Bering Sea: Spatial and temporal variations and factors affecting chlorophyll a concentrations. Deep-Sea Res. II 134, 100–114. http://dx.doi.org/10.1016/j.dsr2.2015.07.012.
Eisner, L.B., Napp, J.M., Pinchuk, A., Andrews, A., 2014. Climate-mediated changes in zooplankton community structure for the eastern Bering Sea. Deep-Sea Res. II 109, 157–171.
Escoffier, N., Bernard, C., Hamlaoui, S., Groleau, A., Catherine, A., 2015. Quantifying plankton communities using spectral fluorescence: the effects of species composition and physiological states. J. Plankton Res. 37, 233–247.
Fissel, B., Dalton, M., Felthoven, R., Garber-Yonts, B., Haynie, A., Himes-Cornell, A., Kasperski, S., Lee, J., Lew, D., Seung, C., 2015. Economic status of the groundfish fisheries off Alaska, 2014. In: Stock assessment and fishery evaluation report for the groundfish resources of the Bering Sea/Aleutian Islands regions. North Pacific Fishery Management Council, 605 W. 4th Avenue, Suite 306, Anchorage, AK 99501.
Friday, N.A., Waite, J.M., Zerbini, A.N., Moore, S.E., 2012. Cetacean distribution and abundance in relation to oceanographic domains on the eastern Bering Sea shelf: 1999-2004. Deep-Sea Res. II 65-70, 260–272.
Friday, N.A., Zerbini, A.N., Waite, J.M., Moore, S.E., Clapham, P.J., 2013. Cetacean distribution and abundance in relation to oceanographic domains on the eastern Bering Sea shelf: 2002, 2008 and 2010. Deep-Sea Res. II 94, 244–256.
Fulton, E.A., 2010. Approaches to end-to-end ecosystem models. J. Mar. Syst. 81, 171–183.
Fulton, E.A., 2011. Interesting times: winners, losers, and system shifts under climate change around Australia. ICES J. Mar. Sci. 68, 1329–1342.
Fulton, E.A., Smith, A.,D.M., Smith, D.C., Johnson, P., 2014. An Integrated approach is needed for ecosystem based fisheries management: Insights from ecosystem-level management strategy evaluation. PLoS One 9 (1), e84242. http://dx.doi.org/10.1371/journal.pone.0084242.
Gibson, G.A., Spitz, Y.H., 2011. Impacts of biological parameterization, initial conditions, and environmental forcing on parameter sensitivity and uncertainty in a marine ecosystem model for the Bering Sea. J. Mar. Syst. 88, 214–231.
Harvey, M., Galbraith, P.S., Descroix, A., 2009. Vertical distribution and diel migration of macrozooplankton in the St. Lawrence marine system (Canada) in relation with the cold intermediate layer thermal properties. Prog. Oceanogr. 80, 1–21.
Harvey, H.R., Pleuthner, R.L., Lessard, E.J., Bernhardt, M.J., Shaw, T.C., 2012. Physical and biochemical properties of the euphausiids *Thysanoessa inermis*, *Thysanoessa raschii*, and *Thysanoessa longipes* in the eastern Bering Sea. Deep-Sea Res. II 65–70, 173–183.
Heintz, R.A., Siddon, E.C., Farley Jr., E.C., Napp, J.M., 2013. Correlation between recruitment and fall condition of age-0 pollock (*Theragra chalcogramma*) from the eastern Bering Sea under varying climate conditions. Deep-Sea Res. II 94, 150–156.
Hermann, A.J., Gibson, G.A., Bond, N.A., Curchitser, E.N., Hedstrom, K., Cheng, W., Wang, M., Cokelet, E.D., Stabeno, P.J., Aydin, K., 2016. Projected future biophysical states of the Bering Sea. Deep-Sea Res. II 134, 30–47. http://dx.doi.org/10.1016/j.dsr2.2015.11.001.
Hermann, A.J., Gibson, G.A., Bond, N.A., Curchitser, E.N., Hedstrom, K., Cheng, W., Wang, M., Stabeno, P.J., Eisner, L., Cieciel, K.D., 2013. A multivariate analysis of observed and modeled biophysical variability on the Bering Sea shelf: multidecadal hindcasts (1970–2009) and forecasts (2010-2040). Deep-Sea Res II 94, 121–139. http://dx.doi.org/10.1016/j.dsr2.2013.04.007.
Hollowed, A.B., Aydin, K.Y., Essington, T.E., Ianelli, J.N., Megrey, B.A., Punt, A.E., Smith, A.D.M., 2011. Experience with quantitative ecosystem assessment tools in the northeast Pacific. Fish and Fisheries, 12; 2011, pp. 189–208.
Hollowed, A.B., Barbeaux, S., Farley, E., Cokelet, E.D., Kotwicki, S., Ressler, P.H., Spital, C., Wilson, C.D., 2012. Effects of climate variations on pelagic ocean habitats and their role in structuring forage fish distributions in the Bering Sea. Deep-Sea Res. II 65–70, 230–250.
Hollowed, A.B., Curchitser, E.N., Stock, C.A., Zhang, C.I., 2013. Trade-offs associated with different modeling approaches for assessment of fish and shellfish responses to climate change. Clim. Change 119, 111–129.
Huenerlage, K., Graeve, M., Buchholz, C., Buchholz, F., 2015. The other krill: overwintering physiology of adult *Thysanoessa inermis* (Euphausiacea) from the high-Arctic Kongsfjord. Aquat. Biol. 23, 225–235.
Hunt Jr., G.L., Allen, B.M., Angliss, R.P., Baker, T., Bond, N., Buck, G., Byrd, G.V., Coyle, K.O., Devol, A., Eggers, D.M., Eisner, L., Feely, R., Fitzgerald, S., Fritz, L.W. Gritsay, E.V., Ladd, C., Lewis, W., Mathis, J., Mordy, C.W., Mueter, F., Napp, J., Sherr, E., Shull, D., Stabeno, P., Stepanenko, M.A., Strom, S., Whitledge, T.E. 2010. Status and trends of the Bering Sea region, 2003–2008, pp 196–267. In: S.M. McKinnell and M.J. Dagg [Eds.] Marine Ecosystems of the North Pacific Ocean, 2003-2008. PICES Special Publication 4, 393 p.
Hunt Jr., G.L., Coyle, K.O., Eisner, L.B., Edward, V., Heintz, R.A., Mueter, F., Napp, J.M., Overland, J.E., Ressler, P.H., Salo, S., Stabeno, P.J., 2011. Climate impacts on eastern Bering Sea foodwebs: a synthesis of new data and an assessment of the Oscillating Control Hypothesis. ICES J. Mar. Sci. 68, 1230–1243.
Hunt Jr., G.L., Renner, M., Kuletz, K., 2014. Seasonal variation in the cross-shelf distribution of seabirds in the southeastern Bering Sea. Deep-Sea Res. II 109, 266–281.
Hunt Jr, G.L., Ressler, P.H., Gibson, G.A., De Robertis, A., Aydin, K., Sigler, M.F., Ortiz, I., Lessard, E.J., Williams, B.C., Pinchuk, A., Buckley, T., 2016. Euphausiids in the eastern Bering Sea: A synthesis of recent studies of euphausiid production, consumption and population control. Deep-Sea Res. II 134, 204–222. http://dx.doi.org/10.1016/j.dsr2.2015.10.007.
Ianelli, J., Holsman, K.K., Punt, A.E., Aydin, K., 2016. Multi-model inference for incorporating trophic and climate uncertainty into stock assessments. Deep-Sea Res. II 134, 379–389. http://dx.doi.org/10.1016/j.dsr2.2015.04.002.
Ianelli, J., Honkahleto, T., Barbeaux, S., Kotwicki, S. Aydin, K., Williamson, N., 2011. Assessment of the walleye pollock stock in the eastern Bering Sea. In: Stock assessment and fishery evaluation report for the groundfish resources of the Bering Sea/Aleutian Islands regions. North Pacific Fishery Management Council, 605 W. 4th Avenue, Suite 306, Anchorage, AK 99501.
Iguchi, N., Ikeda, T., 2004. Vertical distribution, population structure and life history of *Thysanoessa longipes* (Crustacea:Euphausiacea) around Yamato rise: central Japan. J. Plankton Res. 26, 1015–1023.
IPCC, 2007. Contribution of Working Group I to the Fourth Assessment Report of the Intergovernmental Panel on Climate Change, 2007, Climate Change 2007: Working Group I: The Physical Science Basis. Cambridge University Press, Cambridge, United Kindgdom and New York, NY, USA, p. 996.

IPCC, 2013. Contribution of Working Group I to the Fifth Assessment Report of the Intergovernmental Panel on Climate Change. In: Stocker, T.F., Qin, D., Plattner, G.K., Tignor, T., Allen, S.K., Boschung, J., Nauels, A., Xia, Y., Bex, V., Midgley, P.M. (Eds.), Climate Change 2013: The Physical Science Basis. Cambridge University Press, Cambridge, United Kingdom and New York, NY, USA, p. 1535.

Jurado-Molina, J., Livingston, P.A., Ianelli, J.N., 2005. Incorporating predation interactions in a statistical catch-at-age model for predator-prey system in the Bering Sea. Can. J. Fish. Aquat. Sci. 62, 1865–1873.

Kinzey, D., Punt, A.E., 2009. Multispecies and single-species models of fish population dynamics: comparing parameter estimates. Nat. Resour. Model 22, 67–104.

Kishi, M.J., Ito, S., Megrey, B.A., Rose, K.A., Werner, F.E., 2011. A review of the NEMURO and NEMURO.FISH models and their application to marine ecosystem investigations. J. Ocean 67, 3–16.

Kishi, M.J., Kashiwai, M., Ware, D.M., Megrey, B.A., Eslinger, D.L., Werner, F.E., Noguchi-Aita, M., Azumaya, T., Fujii, M., Hashimoto, S., Huang, D., Iizumi, H., Ishida, Y., Kang, S., Kantakov, G.A., Kim, H.-C., Komatsu, K., Navrotsky, V.V., Smith, S.L., Tadokoro, K., Tsuda, A., Yamamura, O., Tamanaka, Y., Yokouchi, K., Yoshie, N., Zhang, J., Zuenko, Y.I., Zvalinsky, V.I., 2007. NEMURO—a lower trophic level model for the North Pacific marine ecosystem. Ecol. Model. 202, 12–25.

Kotwicki, S., Buckley, T., Honkahleto, T., Walters, G., 2005. Variation in the distribution of walleye pollock (*Theragra chalcogramma*) with temperature and implications for seasonal migration. Fish. Bull. 103, 574–587.

Kotwicki, S., Horne, J.K., Punt, A.E., Ianelli, J.N., 2015. Factors affecting the availability of walleye pollock to acoustic and bottom trawl survey gear. ICES J. Mar. Sci. 72, 1425–1439.

Lauth, R., Kotwicki, S., 2013. Detecting temporal trends and environmentally-driven changes in the spatial distribution of bottom fishes and crabs in the eastern Bering Sea shelf. Deep-Sea Res. II 94, 231–243.

Large, W.G., Yeager, S.G., 2009. The global climatology of an interannually varying air-sea 1009 flux data set. Clim. Dyn. 33, 341–364.

Livingston, P.A., Aydin, K., Boldt, J., Ianelli, J., Jurado-Molina, J., 2005. A framework for ecosystem impacts assessment using an indicator approach. ICES J. Mar. Sci. 62, 592–597.

Livingston, P.A., Methot, R.D., 1998. Incorporation of predation into a population assessment model of eastern Bering Sea walleye pollock. P. 663-678. In: Proceedings of the Fishery Stock Assessment Models. Alaska Sea Grant College Program Publication AK-SG-98-01. p. 1037.

Lomas, M.W., Moran, S.B., Casey, J.R., Bell, D.W., Tiahlo, Whitefield, J., Kelly, R.P., Mathis, J.T., Cokelet, E.D., 2012. Spatial and seasonal variability of primary production on the eastern Bering Sea shelf. Deep-Sea Res. II 65–70, 126–140.

Luchin, V., Panteleev, G., 2014. Thermal regimes of the Chukchi Sea from 1941 to 2008. Deep-Sea Res. II 109, 14–26.

Moffitt, E., Punt, A.E., Holsman, K., Aydin, K.Y., Ianelli, J.N., Ortiz, I., 2016. Moving towards ecosystem-based fisheries management: Options for parameterizing multi-species biological reference points. Deep-Sea Res. II 134, 350–359. http://dx.doi.org/10.1016/j.dsr2.2015.08.002.

Morata, N., Søreide, J.E., 2015. Effect of light and food on the metabolism of the Arctic copepod *Calanus glacialis*. Polar Biol. 38, 67–73.

Mordy, C.W., Eisner, L.B., Proctor, P., Stabeno, P., Devol, A.H., Shull, D.H., Napp, J.M., Whitledge, T., 2010. Temporary uncoupling of the marine nitrogen cycle: accumulation of nitrite on the Bering Sea shelf. Mar. Chem. 121, 157–166.

Mueter, F.J., Litzow, M.A., 2008. Sea ice retreat alters the biogeography of the Bering Sea continental shelf. Ecol. Appl. 18, 309–320.

Niebauer, H.J., Alexander, V., Henrich, S.M., 1995. A time-series study of the spring bloom at the Bering Sea-ice edge I: physical processes, chlorophyll and nutrient chemistry. Cont. Shelf Res 15, 1859–1877.

North Pacific Fishery Management Council (NPFMC). 2009. Stock assessment and fishery evaluation report for the groundfish fisheries of the Gulf of Alaska and Bering Sea/Aleutian Islands area: Economic status of the Groundfish fisheries off Alaska, 2012. North Pacific Fishery Management Council 605 West 4th Ave., Suite 306 Anchorage, AK 99501.

Orlova, E.M., Dolgov, A.V., Renaud, P.E., Greenacre, M., Halsband, C., Ivshin, V.A., 2014. Climatic and ecological drivers of euphausiid community structure vary spatially in the Barents Sea: relationships from a long time series (1952–2009). Front. Mar. Sci. 1, 1–13. http://dx.doi.org/10.3389/fmars.2014.00074.

Ortiz, I., Wiese, F., Greig, A., 2013. Marine Regions Boundary Data for the Bering Sea Shelf and Slope, Version 1.0. UCAR/NCAR - Earth Observing Laboratory. http://dx.doi.org/10.5065/D6DF6P6C.

Overland, J.E., Salo, S.A., Kantha, L.H., Clayson, C.A., 1999. Thermal stratification and mixing in the Bering Sea shelf. pp.129-215. In: Loughlin, T.R., Ohtani, K., (Eds.) 1999. Dynamics of the Bering Sea. University of Alaska Sea Grant, AK-SG-99-03, Fairbanks, 838 p.

Page, L.M., Espinosa-Pérez, H., Findley, L.T., Gilbert, C.R., Lea, R.N., Mandrak, N.E., Mayden, R.L., Nelson, J.S., 2013. Common and scientific names of fishes from the United States, Canada, and Mexico, 7th edn. Spec. Publ. Am. Fish. Soc. No. 34, Bethesda, MD. 243 pp.

Petrik, C.M., Duffy-Anderson, J.T., Mueter, F., Hedstrom, K., Curchitser, E.N., 2015. Biophysical transport model suggests climate variability determines distribution of Walleye Pollock early life stages in the eastern Bering Sea through effects on spawning. Prog. Oceanogr. 138, 459–474.

Punt, A.E., Ortiz, I., Aydin, K., Hun Jr, G.L., Wiese, F.K., 2016. End-to-end modeling as part of an integrated research program in the Bering Sea. Deep-Sea Res. II 134, 413–423. http://dx.doi.org/10.1016/j.dsr2.2015.04.018.

Ressler, P.H., De Robertis, A., Kotwicki, S., 2014. The spatial distribution of euphausiids and walleye pollock in the eastern Bering Sea does not imply top-down control by predation. Mar. Ecol. Prog. Ser. 503, 111–222.

Ressler, P.H., De Robertis, A., Warren, J.D., Smith, J.N., Kotwicki, S., 2012. Developing an acoustic survey of euphausiids to understand trophic interactions in the Bering Sea ecosystem. Deep-Sea Res. II 65–70, 184–195.

Rho, T., Whitledge, T.E., 2007. Characteristics of seasonal and spatial variations of primary production over the southeastern Bering Sea shelf. Cont. Shelf Res 27, 2556–2569.

Rose, K.A., Allen, J.I., Artioli, Y., Barange, M., Blackford, J., Carlotti, F., Cropp, R., Daewell, U., Edwards, K., Flynn, K., Hill, S.,L., HilleRisLambers, R., Huse, G., Mackinson, S., Megrey, B., Moll, A., Rivkin, R., Salihoglu, B., Schrum, C., Shannon, L., Shin, Y., Smith, S.L., Smith, C., Solidoro St., C., John, M., Zhou, M., 2010. End-to-end modeling for the analysis of marine ecosystems: challenges, issues and next steps. Mar. Coast. Fish. 2, 115–130.

Rose, K.A., Fiechter, J., Curchitser, E.N., Hedstrom, K., Bernal, M., Creekmore, S., Haynie, A., Ito, S., Lluch-Cota, S., Megrey, B.A., Edwards, C.A., Checkley, D., Koslow, T., McClatchie, S., Werner, F., MacCall, A., Agostini, V., 2015. Demonstration of a fully-coupled end-to-end model for small pelagic fish using sardine and anchovy in the California Current. Prog. Oceanogr. 138, 348–380.

Russel, R.W., Harrison, N.M., Hunt Jr., G.L., 1999. Foraging at a front: hydrography, zooplankton and avian planktivory in the northern Bering Sea. Mar. Ecol. Prog. Ser. 182, 77–93.

Saha, S., Moorthi, S., Pan, H.-L., Wu, X., Wang, J., Nadiga, S., Tripp, P., Kistler, R., Woollen, J., Behringer, D., Liu, H., Stokes, D., Grumbine, R., Gayno, G., Wang, J., Hou, Y.-T., Chuang, H.-Y., Juang, H.-M.H., Sela, J., Iredell, M., Treadon, R., Kleist, D., Van Delst, P., Keyser, D., Derber, J., Ek, M., Meng, J., Wei, H., Yang, R., Lord, S., Van Den Dool, H., Kumar, A., Wang, W., Long, C., Chelliah, M., Xue, Y., Hunag, B., Schemm, J.-K., Ebisuzaki, W.,C.-Z., Liu, Q., Chen, Y., Han, Y., Cucurull, L., Reynolds, R.W., Rutledge, G., Goldberg, M., 2010. The NCEP climate forecast system reanalysis. Bull. Am. 91, 1015–1057. http://dx.doi.org/10.1175/2010BAMS3001.1.

Salinger, M.J., 2013. A brief introduction to the issue of climate and marine fisheries. Clim. Change 119, 23–35.

Salomone, P., Morstad, S., Sands, T., Jones, M., Baker, T., Buck, G., West, F., Kerig, T., 2011. 2010 Bristol Bay Area Annual Management Report, pp. 11–23. ⟨http://www.adfg.alaska.gov/FedAidpdfs/FMR11-23.pdf⟩.

Sargent, J.R., Falk-Petersen, S., 1981. Ecological investigations on the zooplankton community in Balsfjorden, northern Norway: lipids and fatty acids in *Meganyctiphanes norvegica*, *Thysanoessa raschi* and *T. inermis* during midwinter. Mar. Biol. 62, 131–137.

Siddon, E.C., Kristiansen, T., Mueter, F.J., Holsman, K.K., Heintz, R.A., Farley, E.V., 2013. Spatial match-mismatch between juvenile fish and prey provides a mechanism for recruitment variability across contrasting climate conditions in the eastern Bering Sea. PLoS One 8 (12), e84526. http://dx.doi.org/10.1371/journal.pone.0084526.

Sigler, M.F., Stabeno, P.J., Eisner, L.B., Napp, J.M., Mueter, F.J., 2014. Spring and fall phytoplankton blooms in a productive subarctic ecosystem, the eastern Bering Sea, during 1995-2011. Deep-Sea Res. II 109, 71–83.

Smith, S.L., 1991. Growth, development and distribution of the euphausiids *Thysanoessa raschii* (M. Sars) and *Thysanoessa inermis* (Krøyer) in the southeastern Bering Sea. Polar Res. 10, 461–478.

Stabeno, P.J., Bond, N.A., Salo, S.A., 2007. On the recent warming of the southeastern Bering Sea shelf. Deep-Sea Res. II 54, 2599–2618.

Stabeno, P.J., Danielson, S.L., Kachel, D.G., Kachel, N.B., Mrdy, C.W., 2016. Currents and transport on the Eastern Bering Sea shelf: An integration of over 20 years of data. Deep-Sea Res. II 134, 13–29. http://dx.doi.org/10.1016/j.dsr2.2016.05.010.

Stabeno, P.J., Hunt Jr, G.L., 2002. Overview of the inner front and southeast Bering Sea carrying capacity programs. Deep-Sea Res. II 49, 6157–6168.

Stabeno, P.J., Farley Jr, E.V., Kachel, N.B., Moore, S., Mordy, C.W., Napp, J.M., Overland, J.E., Pinchuk, A.I., Sigler, M.F., 2012a. A comparison of the physics of the northern and southern shelves of the eastern Bering Sea and some implications for the ecosystem. Deep-Sea Res. II. 65, 14–30.

Stabeno, P.J., Kachel, N.B., Moore, S.E., Napp, J.M., Sigler, M., Yamaguchi, A., Zerbini, A.N., 2012b. Comparison of warm and cold years on the southeastern Bering Sea shelf and some implications for the ecosystem. Deep-Sea Res. II. 65, 31–45.

Stabeno, P., Napp, J., Mordy, C., Whitledge, T., 2010. Factors influencing physical structure and lower trophic levels of the eastern Bering Sea shelf in 2005: Sea-ice, tides and winds. Prog. Oceanogr. 85, 80–196.

Stabeno, P.J., Schumacher, J.D., Davis, R.F., Napp, J.M., 1998. Under-ice observations of water column temperature, salinity and spring phytoplankton dynamics: eastern Bering Sea shelf. J. Mar. Res. 56, 239–255.

Sullivan, M.E., Kachel, N.B., Mordy, C.W., Salo, S.A., Stabeno, P.J., 2014. Sea-ice and water column structure on the eastern Bering Sea shelf. Deep-Sea Res. II 109, 39–56.

Travers, M., Shin, Y.J., Jennings, S., Cury, P., 2007. Towards end-to-end models for investigating the effects of climate and fishing in marine ecosystems. Prog. Oceanogr. 75, 751–770.

Travers, M., Shin, Y.J., Jennings, S., Machu, E., Huggett, J.A., Field, J.G., Cury, P.M., 2009. Two-way coupling versus one-way forcing of plankton and fish models to predict ecosystem changes in the Benguela. Ecol. Model. 220, 3089–3099.

Travers-Trolet, M., Shin, Y.-J., Field, J.G., 2014a. An end-to-end coupled model ROMS-N2P2Z2D2-OSMOSE of the southern Benguela foodweb: parameterisation, calibration and pattern-oriented validation. Afr. J. Mar. Sci. 36, 11–29.

Travers-Trolet, M., Shin, Y.-J., Shannon, L.J., Moloney, C.L., Field, J.G., 2014b. Combined fishing and climate forcing in the Southern Benguela upwelling ecosystem: an end-to-end modelling approach reveals dampened effects. PLoS One 9, E94286.

Tsuda, A., Saito, H., Kasai, H., 2001. Life history strategies of subarctic copepods *Neocalanus flemingeri* and *N. plumchrus*, especially concerning lipid accumulation patterns. Plankton Biol. Ecol. 48, 52–58.

Vidal, J., Smith, S.L., 1986. Biomass, growth, and development of populations of herbivorous zooplankton in the southeastern Bering Sea during spring. Deep-Sea Res. II 33, 523–556.
Ware, D.M., 1978. Bioenergetics of pelagic fish: theoretical change in swimming speed and ration with body size. J. Fish. Res. Board Can. 35, 220–228.
Wang, J., Hu, H., Mizobata, K., Saito, S.-I., 2009. Seasonal variations of sea-ice and ocean circulation in the Bering Sea: a model-data fusion study. J. Geophys. Res. 114, C02011. http://dx.doi.org/10.1029/2008JC004727.
Wiese, F.K., Wiseman Jr., W.J., Van Pelt, T.I., 2012. Bering sea linkages. Deep-Sea Res. II. 65-70, 2–5.
Witherell, D., Pautzke, C.P., Fluharty, D., 2000. An ecosystem-based approach for Alaska groundfish fisheries. ICES J. Mar. Sci. 57, 771–777.
Wyllie-Echeverria, T., Wooster, W.S., 1998. Year-to-year variations in Bering Sea-ice cover and some consequences for fish distributions. Fish. Oceanogr. 7, 1063–1074.
Zador, S. (Ed). 2015. Ecosystem consideration 2015. North Pacific Fishery Management Council 605 West 4th Ave., Suite 306 Anchorage, AK 99501. 297 p. ⟨https://www.afsc.noaa.gov.REFM/Docs/2015/ecosystem.pdf⟩.